

# Study of ground state properties of carbon isotopes with deformed relativistic Hartree-Bogoliubov theory in continuum

Xiang-Xiang Sun<sup>a,b</sup>, Jie Zhao<sup>c</sup>, Shan-Gui Zhou<sup>a,b,d,e,\*</sup>

<sup>a</sup>*CAS Key Laboratory of Theoretical Physics, Institute of Theoretical Physics, Chinese Academy of Sciences, Beijing 100190, China*

<sup>b</sup>*School of Physical Sciences, University of Chinese Academy of Sciences, Beijing 100049, China*

<sup>c</sup>*Center for Quantum Computing, Peng Cheng Laboratory, Shenzhen 518055, China*

<sup>d</sup>*Center of Theoretical Nuclear Physics, National Laboratory of Heavy Ion Accelerator, Lanzhou 730000, China*

<sup>e</sup>*Synergetic Innovation Center for Quantum Effects and Application, Hunan Normal University, Changsha 410081, China*

---

## Abstract

Ground state properties of carbon isotopes, including root-mean-square radii, neutron separation energies, single particle spectra, and shapes are systematically studied with the deformed relativistic Hartree-Bogoliubov theory in continuum. The calculations with the effective interaction PK1 reproduce the available data reasonably well. The shell evolution in this isotopic chain is investigated by examining the single particle spectra. The inversion of neutron orbitals  $\nu 2s_{1/2}$  and  $\nu 1d_{5/2}$  compared with the order of neutron orbitals in stable nuclei is revealed in  $^{15-20,22}\text{C}$  when these nuclei are constrained to spherical shape. Neutron halos in  $^{15,19,22}\text{C}$  are studied in detail and their halo structures are mainly caused by the inversion of  $(\nu 2s_{1/2}, \nu 1d_{5/2})$  and deformation effects. In particular,  $^{15}\text{C}$  and  $^{22}\text{C}$  are deformed halo nuclei with shape decoupling effects in ground states.

**Keywords:** Carbon isotopes, deformed halo,  $(\nu 2s_{1/2}, \nu 1d_{5/2})$  inversion, shape decoupling, deformed RHB theory in continuum

---



---

\*Corresponding author.

Email address: [sgzhou@itp.ac.cn](mailto:sgzhou@itp.ac.cn) (Shan-Gui Zhou )

## 1. Introduction

Many interesting and exotic nuclear phenomena have been observed or predicted in carbon isotopes, including neutron halos, cluster structures, new magicities, shape decoupling effects, etc. As far as neutron halos are concerned,  $^{15,19}\text{C}$  are one-neutron halo nuclei [1, 2] and  $^{22}\text{C}$  is the heaviest two-neutron halo nucleus with a Borromean structure so far [3, 4]. They are all weakly bound, characterized by small one(two)-neutron separation energies, and have larger radii than neighboring isotopes. One-neutron separation energies of  $^{15}\text{C}$  and  $^{19}\text{C}$  are  $1.1895 \pm 0.0008$  MeV and  $0.5633 \pm 0.0915$  MeV in AME2016 [5–7] respectively. The two-neutron separation energy has not been well determined for  $^{22}\text{C}$  up to now. In 2012,  $S_{2n}(^{22}\text{C})$  was deduced to be  $-0.14 \pm 0.46$  MeV from direct mass measurements [8]. The empirical value of the two-neutron separation energy for  $^{22}\text{C}$  is  $110 \pm 60$  keV in AME2012 [9–11] and  $35 \pm 20$  keV in AME2016 [5–7]. The matter and proton radii of  $^{12-19}\text{C}$  have been reported in Ref. [12] where the feature of one-neutron halo in  $^{15}\text{C}$  and  $^{19}\text{C}$  was illustrated. The matter radius of  $^{22}\text{C}$  was deduced from two interaction cross section measurements [3, 4]; the two deduced values differ very much:  $R_m = 5.4 \pm 0.9$  fm in 2010 [3] and  $R_m = 3.44 \pm 0.08$  fm in 2016 [4]. More recently, a new value,  $R_m(^{22}\text{C}) = 3.38 \pm 0.10$  fm, much smaller than the one given in 2010 [3] but close to the result in 2016, was obtained by using a Glauber model [13].

Nuclear halos are formed because of a considerably large occupation of  $s$ - or  $p$ -orbitals close to the threshold of the neutron or proton emission in weakly bound systems. Neutron halos in carbon isotopes are mainly caused by the loosely bound  $s$ -orbital [3, 4, 14], the energy and occupation of which are closely related to the shell evolution and changes of nuclear magicities [15–18] along this isotopic chain. A new proton magic number  $Z = 6$  in  $^{13-20}\text{C}$  was explored in Ref. [19]; if this is the case,  $^{14}\text{C}$  would be a doubly-magic nucleus with magic numbers  $Z = 6$  and  $N = 8$ . The neutron orbital  $\nu 2s_{1/2}$  is lower than  $\nu 1d_{5/2}$  in  $^{15}\text{C}$ , as pointed out in Ref. [14]. That is,  $\nu 2s_{1/2}$  and  $\nu 1d_{5/2}$  are inverted as compared with single particle levels in stable nuclei. This inversion results in the formation of a one-neutron halo in this nucleus. For  $^{16,18,20}\text{C}$ , the ground state configurations are mixtures of  $(\nu 2s_{1/2}, \nu 1d_{5/2})$  and there is no shell gap at  $N = 14$  in  $^{20}\text{C}$  [20].  $^{22}\text{C}$  is the key nucleus to understand whether the shell closure at  $N = 16$  [20–22] appears or not in this isotopic chain, which is related to the competition between  $\nu 2s_{1/2}$  orbital and  $\nu 1d_{5/2}$  orbital [18, 22–31]; this competition also

determines the halo configuration in  $^{22}\text{C}$ . In addition, it is worth mentioning that the cluster structure has been a very hot topic in carbon isotopes, such as  $3\alpha$  configuration in the Hoyle state of  $^{12}\text{C}$  [32–35],  $3\alpha+xn$  cluster structure in  $^{13,14,16}\text{C}$  [36–44], and rod shapes under high spin and isospin [44, 45].

There have been several systematic theoretical studies on ground state properties of carbon isotopes. Calculations made by using a spherical relativistic Hartree-Bogoliubov (SRHB) theory with the effective interaction NL3 indicated no halos in carbon isotopes [46]. With the Fock term included, the spherical relativistic Hartree-Fock-Bogoliubov (SRHFB) theory has shown one-neutron halo structure in  $^{17,19}\text{C}$  but no halo in  $^{22}\text{C}$  [47]. These SRHB and SRHFB calculations [46, 47] were carried out in coordinate space with spherical symmetry imposed. Investigations have been made by using covariant density functional theories [48–52] or Skyrme density functional theories [53–55] with deformation effects considered. It has been shown that intrinsic deformations in ground states of carbon isotopes have a strong dependence on the number of neutrons. There are also some shell model studies [30, 40, 56] aiming at the description of shell evolution and related properties in carbon isotopes.

When combining together the halo structure, shell evolution, and deformation effects, more complex and exotic nuclear phenomenon appears [57]. One typical example is  $^{22}\text{C}$  in which the interplay among the halo feature, shell evolution, and deformation effects has been revealed [58] by using the deformed relativistic Hartree-Bogoliubov theory in continuum (the DRHBc theory). The DRHBc theory can self-consistently describe ground state properties including the halo, evolution of single particle spectrum, and shell structure with deformation effects considered [59–64]. In Ref. [58], the uncertainties or puzzles on the matter radius and the halo configuration of  $^{22}\text{C}$  are resolved and the “shrunk” halo feature is attributed to the inversion of  $\nu 2s_{1/2}$  and  $\nu 1d_{5/2}$  and deformation effects.  $^{22}\text{C}$  was predicted to be a candidate of deformed halo nucleus with shape decoupling effects, i.e., the core and the halo have different shapes. The shape decoupling in deformed nuclei has been widely investigated by using the DRHBc theory [59, 60] and Hartree-Fock-Bogoliubov theories with the Skyrme interaction [65–68] and the M3Y-type semirealistic interaction [69, 70] for axially deformed nuclei.

In this paper we present a systematic study of bulk properties, including separation energies, matter radius, and deformations, of this isotopic chain by using the DRHBc theory. We focus on halo structures, deformation effects, and the evolution of single neutron levels with quadrupole deformation. The

paper is organized as follows. The main formulae of the DRHBc theory are displayed in Sec. 2. The results and discussions of bulk properties of carbon isotopes are given in Sec. 3. The structure of odd  $A$  nuclei  $^{15,17,19}\text{C}$  is discussed in Sec. 4. The results for  $^{22}\text{C}$  from DRHBc calculations are shown in Sec. 5. In Sec. 6 we summarize this work.

## 2. The DRHBc theory

The covariant density function theory (CDFT) is one of the most successful models for the study of nuclear structure in almost the whole nuclear landscape [62, 71–79]. The relativistic continuum Hartree-Bogoliubov (RCHB) theory [80, 81] and the DRHBc theory [59, 60] have been developed and used to study ground state properties of spherical and deformed halo nuclei, respectively. The detailed formulae for the DRHBc theory can be found in Refs. [59–61, 82]. Here we give briefly the main ones for convenience of discussions in the following sections. The relativistic Hartree-Bogoliubov (RHB) equation for nucleons [83] reads,

$$\begin{pmatrix} h_D - \lambda_\tau & \Delta \\ -\Delta^* & -h_D^* + \lambda_\tau \end{pmatrix} \begin{pmatrix} U_k \\ V_k \end{pmatrix} = E_k \begin{pmatrix} U_k \\ V_k \end{pmatrix}, \quad (1)$$

which is solved in a spherical Dirac Woods-Saxon (WS) basis [84].  $E_k$  is the quasi particle energy,  $\lambda_\tau$  ( $\tau = \text{n, p}$ ) is the chemical potential, and  $U_k$  and  $V_k$  are quasi particle wave functions.  $h_D$  is the Dirac Hamiltonian

$$h_D = \boldsymbol{\alpha} \cdot \mathbf{p} + V(\mathbf{r}) + \beta[M + S(\mathbf{r})], \quad (2)$$

where  $S(\mathbf{r})$  and  $V(\mathbf{r})$  are scalar and vector potentials. The pairing potential reads

$$\Delta(\mathbf{r}_1, \mathbf{r}_2) = V^{pp}(\mathbf{r}_1, \mathbf{r}_2)\kappa(\mathbf{r}_1, \mathbf{r}_2), \quad (3)$$

where we use a density dependent zero-range force in the particle-particle ( $pp$ ) channel,

$$V^{pp}(\mathbf{r}_1, \mathbf{r}_2) = \frac{1}{2}V_0(1 - p^\sigma)\delta(\mathbf{r}_1, \mathbf{r}_2) \left(1 - \frac{\rho(\mathbf{r}_1)}{\rho_{\text{sat}}}\right), \quad (4)$$

and  $\kappa(\mathbf{r}_1, \mathbf{r}_2)$  is the pairing tensor [85, 86].

For axially deformed nuclei with spatial reflection symmetry, we expand scalar densities and potentials in terms of Legendre polynomials,

$$f(\mathbf{r}) = \sum_{\lambda} f_{\lambda}(r) P_{\lambda}(\cos \theta), \quad \lambda = 0, 2, 4, \dots, \quad (5)$$

with

$$f_{\lambda}(r) = \frac{2\lambda + 1}{4\pi} \int d\Omega f(\mathbf{r}) P_{\lambda}(\cos \theta). \quad (6)$$

The ground state of an even-even nucleus is obtained by solving the RHB equation iteratively. For systems with odd number of neutrons (protons), the ground state is obtained by taking the blocking effect into account. The details about how to deal with the blocking effect in the DRHBc theory can be found in Ref. [61].

In order to get the potential energy curve and examine the evolution of single particle levels with deformation, one can make constraint calculations [85]. The augmented Lagrangian method [87] has been implemented in the DRHBc theory and the constrained Dirac Hamiltonian  $h'_D$  is written as

$$h'_D = h_D + c_1 \left( \langle \hat{Q}_2 \rangle - \bar{Q}_2 \right) + c_2 \left( \langle \hat{Q}_2 \rangle - \bar{Q}_2 \right)^2, \quad (7)$$

where  $c_1$  is the Lagrange multiplier,  $c_2$  is the penalty parameter, and  $\bar{Q}_2$  is the desired expectation value of the quadrupole moment  $\hat{Q}_2$ . In the iteration,  $c_2$  is kept as a constant and  $c_1$  in the  $m$ th step is re-adjusted in the following way,

$$c_1^{(m)} = c_1^{(m-1)} - 2c_2 \left( \langle \hat{Q}_2 \rangle^{(m-1)} - \bar{Q}_2 \right). \quad (8)$$

The bulk properties of a nucleus in question, including the binding energy, radius, deformation, etc., can be calculated from quasi-particle wave functions and densities [60]. The densities are important for the study of halo nuclei. Next we briefly discuss how to calculate the densities with emphasis on odd  $A$  systems.

The halo is mainly determined by occupation probabilities and wave functions of weakly bound orbitals [88]. For odd  $A$  nuclei, the occupation probability of the blocked level is around 0.5. The neutron (proton) density of an odd  $N(Z)$  nucleus is calculated as [61]

$$\rho(\mathbf{r}) = \sum_{k \neq k_b} |V_k(\mathbf{r})|^2 + |U_{k_b}(\mathbf{r})|^2. \quad (9)$$

The density of a halo nucleus extends far away from the center of the nucleus, which is determined by the asymptotic behavior of the wave function of the valence nucleon(s). For a bound system, the Fermi surface  $\lambda_\tau < 0$  and the asymptotic behavior of quasi particle wave functions  $V_k(r)$  and  $U_k(r)$  are derived as [88, 89]

$$V_k(r) \propto \frac{\exp(-\kappa_{k+}r)}{r}, \quad (10)$$

$$U_k(r) \propto \frac{\exp(-\kappa_{k-}r)}{r}, \quad (11)$$

where  $\kappa_{k\pm} = \sqrt{2m(|\lambda_\tau| \pm E_k)}$ ,  $E_k = \sqrt{(\varepsilon_k - \lambda_\tau)^2 + \Delta_k^2}$  is the quasi particle energy, and  $\varepsilon_k$  and  $\Delta_k$  denote the single particle energy and pairing gap.  $\Delta_k$  stays finite or equals zero, so  $|U_k(r)|^2$  diminishes more slowly to zero with  $r$  than  $|V_k(r)|^2$ . Therefore, the asymptotic behavior of  $U_k(\mathbf{r})$  leads to a more extended density distribution [70] for odd  $A$  nuclei, thus enhancing the formation of a halo.

### 3. Bulk properties of carbon isotopes

We have investigated bulk properties of carbon isotopes by using the DRHBc theory. The two commonly used and successful effective interactions PK1 [90] and NL3 [91] are adopted in the particle-hole ( $ph$ ) channel while a density dependent zero-range pairing force (4) is used in the  $pp$  channel. In this work, the Dirac WS basis is generated in a box with the size  $R_{\text{box}}$  fixed to be 25 fm and the mesh size  $\Delta r = 0.1$  fm. An energy cutoff  $E_{\text{cut}}^+ = 100$  MeV is made to determine the Dirac WS basis for positive-energy states in the Fermi sea and the number of negative-energy states in the Dirac sea is taken the same as that of positive-energy states [60, 84]. A cutoff on the angular momentum is made up to  $J_{\text{max}} = \frac{21}{2}\hbar$ . The pairing strength  $V_0$  and cut-off energy  $E_{\text{cut}}^{\text{q.p}}$  in the quasi-particle space are 355 MeV·fm<sup>3</sup> and 60 MeV respectively, which are the same as in Ref. [58]. The maximal order  $\lambda_{\text{max}}$  in the Legendre expansion (5) is taken to be 4. The ground states of odd  $A$  carbon isotopes are calculated with blocking effects considered. For each odd- $A$  nucleus, we block several single particle levels around the neutron Fermi surface and take the one with maximal binding energy as the ground state.

Table 1: Experimental and calculated neutron separation energy ( $S_{2n}$  for even  $A$  and  $S_n$  for odd  $A$  nuclei), rms matter radius  $R_m$ , and quadrupole deformation parameter  $\beta_2$ .  $\Omega^\pi$  represents the blocked level for each odd  $A$  nucleus. Experimental (Expt.) values of  $S_{2n}$  ( $S_n$ ),  $R_m$ , and  $\beta_2$  are taken from Refs. [7, 12, 92], respectively, except otherwise noted.

$\Omega^\pi$		$S_{2n}$ ( $S_n$ ) (MeV)	$R_m$ (fm)	$\beta_2$
$^{12}\text{C}$	Expt.	31.0950(1)	2.35(2)	0.583(15)
				-0.40(2) [93]
	PK1	31.1020	2.37	-0.3223
	NL3	30.1811	2.25	0.0000
$^{13}\text{C}$	Expt.	4.8304	2.28(4)	
	1/2 <sup>-</sup> PK1	7.7551	2.41	0.0000
	1/2 <sup>-</sup> NL3	7.5501	2.40	0.0000
$^{14}\text{C}$	Expt.	12.8152	2.33(7)	
	PK1	16.8611	2.48	0.0000
	NL3	16.5401	2.49	0.0000
$^{15}\text{C}$	Expt.	1.1895(8)	2.54(4)	
	1/2 <sup>+</sup> PK1	1.2162	2.64	0.2559
	1/2 <sup>+</sup> NL3	1.5832	2.65	0.2510
	5/2 <sup>+</sup> PK1	0.9584	2.60	-0.1746
	5/2 <sup>+</sup> NL3	1.1309	2.62	-0.1647
$^{16}\text{C}$	Expt.	5.3402(35)	2.74(3)	0.323(18)
				0.356 <sup>+0.25</sup> <sub>-0.23</sub> [94]
	PK1	4.4421	2.70	-0.2260
	NL3	5.8507	2.71	-0.1727
$^{17}\text{C}$	Expt.	0.7164(137)	2.76(3)	0.52(4) [95]
	3/2 <sup>+</sup> PK1	1.9631	2.81	0.4621
	3/2 <sup>+</sup> NL3	1.3016	2.83	0.4611
	1/2 <sup>+</sup> PK1	1.4245	2.85	-0.3279
	1/2 <sup>+</sup> NL3	1.3316	2.86	-0.2886
$^{18}\text{C}$	Expt.	4.8022(295)	2.86(4)	0.289 <sup>(+20)</sup> <sub>(-13)</sub>
	PK1	5.2768	2.89	-0.3763
	NL3	5.7614	2.90	-0.3514
$^{19}\text{C}$	Expt.	0.5633(915)	3.16(7)	0.29(3) [95]

$\Omega^\pi$		$S_{2n}$ ( $S_n$ ) (MeV)	$R_m$ (fm)	$\beta_2$
			$3.10(^{+5}_{-3})$ [4]	
$1/2^+$	PK1	0.0304	3.05	0.3743
$3/2^+$	PK1	1.6046	3.02	-0.4459
$3/2^+$	NL3	0.9845	3.02	-0.4395
$^{20}\text{C}$	Expt.	2.9116(2449)	2.98(5) [4]	$0.405(^{+89}_{-45})$
	PK1	2.9014	3.07	-0.4661
	NL3	4.3989	3.07	-0.4098
$^{22}\text{C}$	Expt.	0.1006(6259)	3.44(8) [4]	
		-0.14(46) [8]	5.4(9) [3]	
			3.38(10) [13]	
	PK1	0.3998	3.25	-0.2649
	NL3	1.9343	3.22	-0.2311

Experimental and calculated neutron separation energies, rms matter radii  $R_m$ , and quadrupole deformation parameters  $\beta_2$  of carbon isotopes are presented in Table 1. For each of these nuclei, there are usually more than one minimum in the potential energy curve. For spherical (deformed) odd  $A$  nuclei, we show the results with blocking one (two) single neutron level(s) around the Fermi surface. In Table 1, one can see the spin and parity of the ground state of  $^{15}\text{C}$  ( $^{19}\text{C}$ ) is  $1/2^+$  ( $3/2^+$ ). For  $^{17}\text{C}$ , the ground state spin-parity is  $J^\pi = 3/2^+$  with PK1 and  $J^\pi = 1/2^+$  with NL3. Next we give detailed discussions about these results.

In Fig. 1(a), the calculated  $S_{2n}$  for even  $A$  nuclei and  $2S_n$  for odd  $A$  nuclei are shown and compared with the data taken from Ref. [7]. The odd-even mass staggering in carbon isotopes can be reproduced by calculations with both parameter sets. The calculated  $S_n$  for  $^{13}\text{C}$  and  $S_{2n}$  for  $^{14}\text{C}$  are larger than experimental values. For other carbon isotopes, calculations reproduce the experiment reasonably well.  $^{22}\text{C}$  is the heaviest Borromean nucleus observed so far. Our calculations can reproduce the Borromean feature [96] of  $^{22}\text{C}$  with PK1 but not NL3: With both effective interactions,  $^{20,22}\text{C}$  are bound;  $^{21}\text{C}$  is unbound with PK1 ( $S_n = -28$  keV) but bound with NL3 ( $S_n = 0.22$  MeV). As mentioned in the Introduction, the separation energy  $S_{2n}$  has not been well determined for  $^{22}\text{C}$  yet:  $110 \pm 60$  keV [11],  $-140 \pm 460$  keV [8], and  $35 \pm 20$  keV [7]. The calculated  $S_{2n}$  of  $^{22}\text{C}$  is 0.40 MeV with PK1 and 1.93 MeV with NL3.



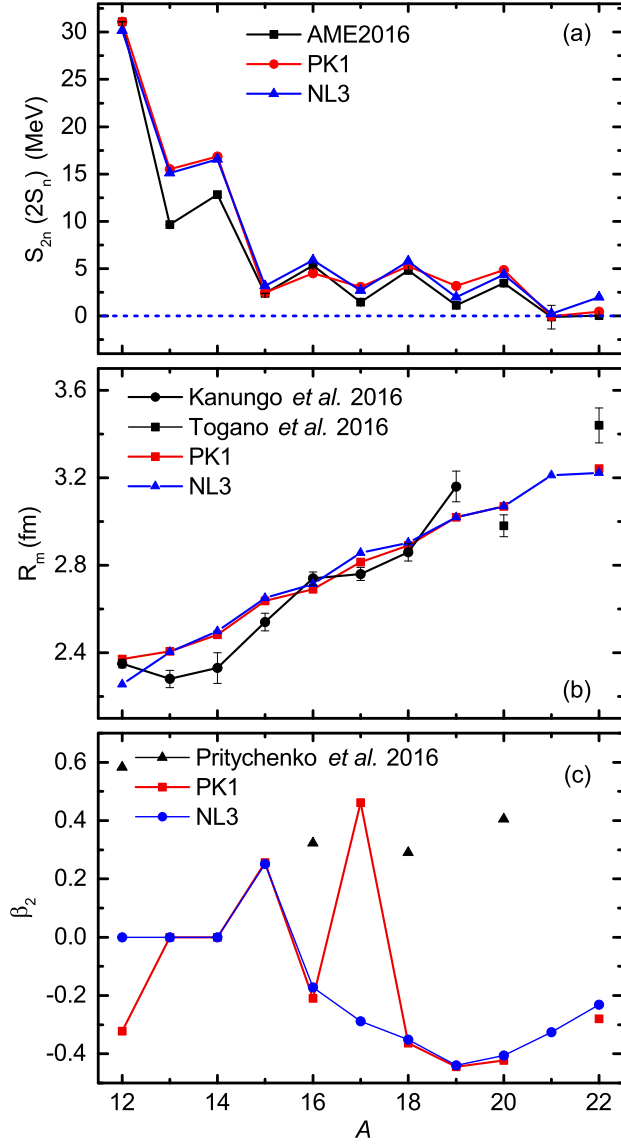


Figure 1: (Color online) (a) Neutrons separation energy  $S_{2n}$  (for even  $A$  nuclei) or  $2S_n$  (for odd  $A$  nuclei), (b) rms matter radius  $R_m$ , and (c) quadrupole deformation parameter  $\beta_2$  for carbon isotopes.

Experimental and calculated rms matter radii  $R_m$  of carbon isotopes are shown in Fig. 1(b). The experimental  $R_m$  values of  $^{12-19}\text{C}$  and  $^{20,22}\text{C}$  are taken from Refs. [4, 12] respectively. The recent progress on the radii of carbon isotopes has been summarized in Ref. [97]. The large enhancement of  $R_m$  with  $A$  is usually regarded as a sign of a halo. One can find such signs at  $A = 15, 19$ , and  $22$  in Fig. 1(b) obviously. There are slightly sudden increases in the calculated  $R_m$  at  $A = 15$  and  $A = 19$ . The calculated  $R_m$  for  $^{15}\text{C}$  with PK1 and NL3 are 2.64 fm and 2.65 fm, a bit larger than the experimental value  $2.54 \pm 0.04$  fm [12].  $R_m$  of  $^{19}\text{C}$  calculated with PK1 and NL3 are both 3.02 fm, which is smaller than experimental values  $3.10^{+0.05}_{-0.03}$  fm [4] and  $3.16 \pm 0.07$  fm [12]. For  $^{20}\text{C}$ , the  $R_m$  values calculated with PK1 and NL3 are both 3.07 fm, slightly larger than the experimental value  $2.97^{+0.03}_{-0.05}$  fm [4]. According to an early experiment,  $^{22}\text{C}$  should be a huge halo nucleus with  $R_m = 5.4 \pm 0.9$  fm [3]. However, much smaller  $R_m$  values were deduced from a more recent measurement of interaction cross sections,  $R_m = 3.44 \pm 0.08$  fm [4] and  $3.38 \pm 0.10$  fm [13]. This means the halo in  $^{22}\text{C}$  was “shrunk”. Our calculated  $R_m$  for  $^{22}\text{C}$ , 3.25 (3.22) fm with PK1 (NL3), is close to these recent experimental results. The mechanism of the shrinkage has been proposed in Ref. [58] and will also be discussed in Sec. 5.

The quadrupole deformation parameters  $\beta_2$  in ground states of nuclei in carbon isotopes are shown in Fig. 1(c). Generally speaking, calculated values of  $\beta_2$  agree with available experimental ones well. In our calculations, the ground state of  $^{12}\text{C}$  is oblate with PK1 but spherical with NL3. The oblate shape of  $^{12}\text{C}$  with PK1 is consistent with an inelastic scattering experiment [93]. A recent experiment [98] confirms the oblate shape of  $^{12}\text{C}$  in its ground state as well. Spherical  $^{13,14}\text{C}$ , prolate  $^{15}\text{C}$ , and oblate  $^{16,18-20,22}\text{C}$  are obtained in calculations with both PK1 and NL3. In a recent work, Jiang et al. studied the quadrupole deformation of  $^{16}\text{C}$  by performing proton and deuteron inelastic scattering experiments [94]. From the  $B(E2; 2_1^+ \rightarrow 0_{\text{g.s.}}^+)$  value ( $4.34^{+2.27}_{-1.85} \text{ e}^2 \text{ fm}^4$ ) given in Ref. [94] one can deduce  $\beta_2 = 0.356^{+0.25}_{-0.23}$  for  $^{16}\text{C}$ . Different shapes are predicted for  $^{17}\text{C}$  in calculations with PK1 (prolate) and NL3 (oblate). Calculations by using Skyrme density functional SkO’ for  $^{17}\text{C}$  predicted a prolate shape in the ground state [99] with the spin-parity  $J^\pi = 3/2^+$ , which agrees with our calculations with PK1. The  $\beta_2$  values of  $^{17}\text{C}$  and  $^{19}\text{C}$  are deduced to be  $0.52 \pm 0.04$  and  $0.29 \pm 0.03$  in Ref. [95]. The intrinsic shape of  $^{16,18}\text{C}$  is prolate and  $^{12,22}\text{C}$  show an oblate shape in the calculation with the MDC-RMF model [51], which agrees with Ref. [53].

The  $\beta_2$  of  $^{22}\text{C}$  with PK1 and NL3 is close to  $-0.25$ , which is similar to results in Refs. [51, 53].

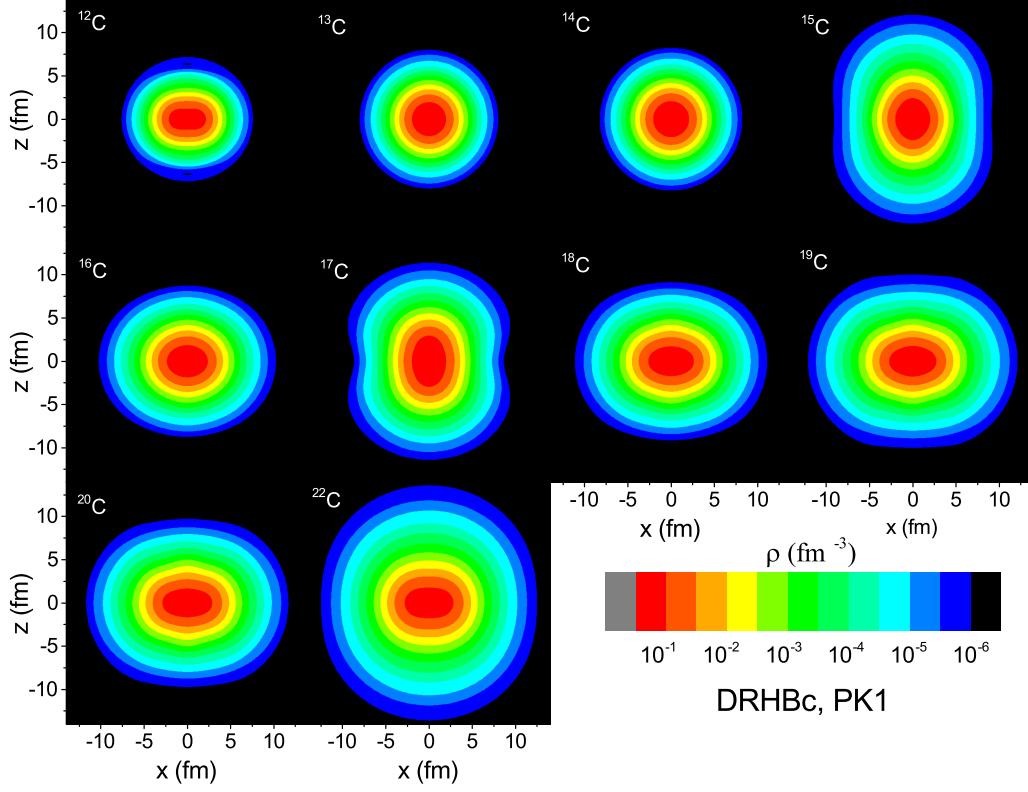


Figure 2: (Color online) Two-dimensional neutron density distributions for  $^{12-20,22}\text{C}$  from DRHBc calculations with PK1. The  $z$ -axis is the symmetry axis for axially deformed systems.

From the above discussions on neutron separation energies, rms matter radii, and deformations for carbon isotopes, it can be seen that the effective interaction PK1 can give a proper description for carbon isotopes. Especially, the Borromean feature of  $^{22}\text{C}$  can be reproduced with PK1. Next we will focus on the results obtained with the parameter set PK1.

In Fig. 2, the two-dimensional neutron density distributions for the ground states of nuclei in this isotopic chain calculated with PK1 are presented. The shape evolution with  $A$  can be clearly seen from these density profiles. Density distributions of  $^{15}\text{C}$  and  $^{22}\text{C}$  have larger spatial extensions

than adjacent isotopes.

Next we discuss the shell evolution in this isotopic chain by investigating single particle spectra. Single neutron spectra for carbon isotopes with even  $A$  are shown in Fig. 3. For each nucleus, quadrupole deformation constraint calculations are carried out to get the single neutron levels versus the deformation parameter  $\beta_2$ . In the spherical case, the neutron orbital  $\nu 2s_{1/2}$  is lower than  $\nu 1d_{5/2}$  for  $^{16,18,20,22}\text{C}$ , which means  $\nu 2s_{1/2}$  and  $\nu 1d_{5/2}$  are inverted compared with the order of neutron orbitals in stable nuclei. Furthermore,  $\nu 2s_{1/2}$  and  $\nu 1d_{5/2}$  are nearly degenerate in these carbon isotopes. The inversion and near degeneracy of  $(\nu 2s_{1/2}, \nu 1d_{5/2})$  lead to the appearance of the magic number  $N = 16$ , corresponding to the large gap between  $\nu 1d_{3/2}$  and  $\nu 1d_{5/2}$ . This inversion in carbon isotopes has also been predicted by using a shell model approach with chiral  $NN$  potential [30]. The shell closure at  $N = 14$  [20, 40, 100] no longer exists in DRHBc calculations with PK1 due to the near degeneracy of  $(\nu 2s_{1/2}, \nu 1d_{5/2})$ . When the deformation comes in, it is more complicated to identify new magic numbers according to single particle levels (SPLs) because of the large level density caused by quadrupole correlations. In  $^{16,18,20,22}\text{C}$ ,  $s$ - and  $d$ -wave orbitals mix strongly due to quadrupole correlations, resulting in deformed ground states. In particular, the magic number  $N = 16$ , which appears in the spherical limit, disappears after taking deformation effects into account in  $^{22}\text{C}$  [58]. The SPLs and configurations of odd  $A$  nuclei  $^{15,17,19}\text{C}$  will be shown and discussed one by one in the next section.

#### 4. Structure of $^{15,17}\text{C}$ and $^{19}\text{C}$

The one-neutron halo structure in  $^{15}\text{C}$  and  $^{19}\text{C}$  has been confirmed experimentally [1, 101].  $^{17}\text{C}$  is not a halo nucleus in the ground state. The experimental results, including the spin-parity  $J^\pi$  of the ground state and valence orbitals for these nuclei, are listed in Table 2. More experimental information can be found in Ref. [14].

Halo nuclei are weakly bound and well associated with pairing correlations and the contribution from the continuum above the threshold of particle emission [14, 80, 81, 108–114]. When valence neutron(s) occupy low  $l$ -orbitals ( $s$ - or  $p$ -wave) close to the threshold, including weakly bound ones and those embedded in the continuum, a halo appears. Single neutron levels of  $^{15,17,19}\text{C}$  and  $^{19}\text{C}^*$  (the halo state corresponding to the second energy minimum in the potential energy surface with the single neutron level  $1/2_3^+$  blocked) in the

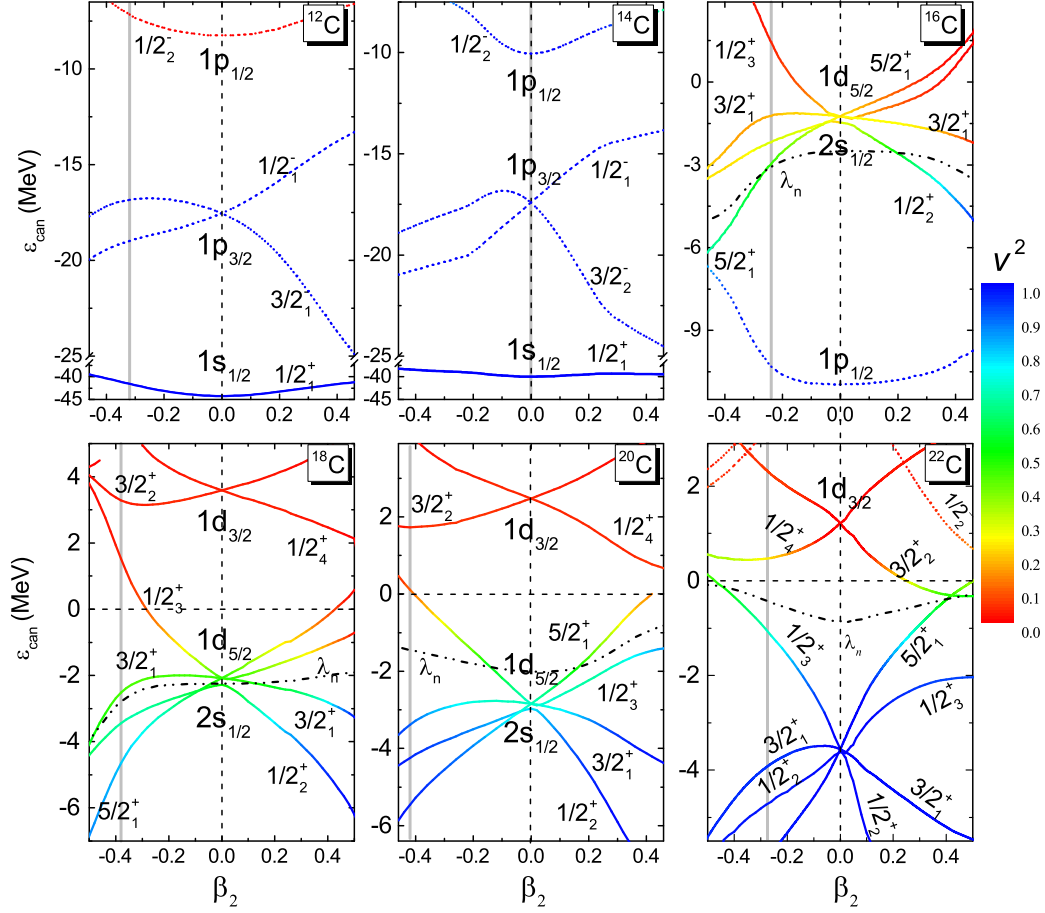


Figure 3: (Color online) Single neutron levels in the canonical basis of  $^{12,14,16,18,20,22}\text{C}$  from deformation constraint DRHBc calculations with PK1. Levels with positive (negative) parity are presented by solid (dotted) lines. Each level is labeled with  $\Omega_i^\pi$  where  $\pi$  is the parity,  $\Omega$  is the projection of the angular momentum on the symmetry axis, and  $i$  is used to order the level in each  $\Omega^\pi$ -block. The occupation probability  $\nu^2$  of each orbital is represented with different colors. The ground state is indicated by the gray vertical line. The Fermi levels ( $\lambda_n$ ) are displayed by black dash-dotted lines. For  $^{12}\text{C}$  and  $^{14}\text{C}$ , all single particle levels shown in the figures are fully occupied and the Fermi levels are not shown.

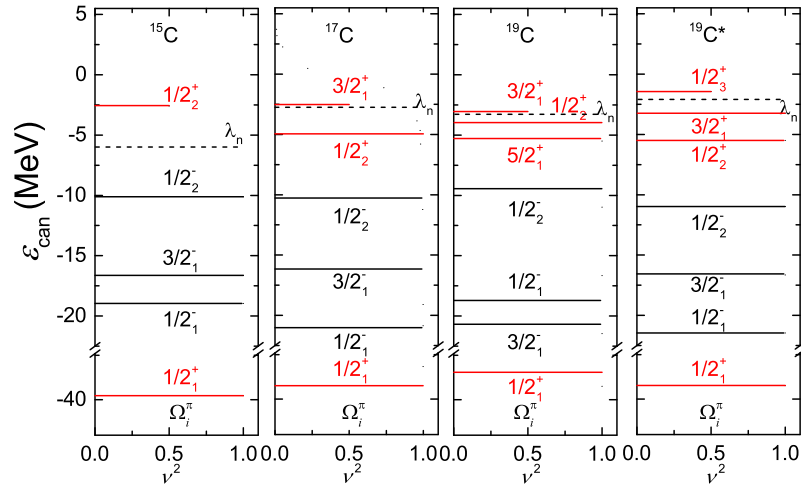


Figure 4: (Color online) Single neutron levels in the canonical basis of  $^{15,17,19}\text{C}$  and  $^{19}\text{C}^*$  from DRHBc calculations with PK1. Each level is labeled with  $\Omega_i^\pi$  where  $\pi$  is the parity,  $\Omega$  is the projection of the angular momentum on the symmetry axis, and  $i$  is used to order the level in each  $\Omega^\pi$ -block. The length of each level is proportional to the occupation probability  $v^2$ . Levels with positive (negative) parity are presented by red (black) lines. The dash line represents the neutron Fermi surface.

Table 2: Experimental ground state spin-parity  $J^\pi$  and valence orbitals of  $^{15,17,19}\text{C}$ .

Nucleus	$J^\pi$ (g.s.)	Valence orbital
$^{15}\text{C}$	$1/2^+$ [2, 102, 103]	<i>s</i> -wave
$^{17}\text{C}$	$3/2^+$ [95, 104, 105]	<i>d</i> -wave
$^{19}\text{C}$	$1/2^+$ [95, 104, 106, 107]	<i>s</i> -wave

canonical basis are given in Fig. 4. In our DRHBc calculations with blocking effects taken into account, pairing gaps of  $^{15,17,19}\text{C}$  and  $^{19}\text{C}^*$  almost vanish and continuum states are empty. Therefore, whether a halo emerges or not in these nuclei is totally determined by the configuration of the weakly bound level and blocked orbitals.

#### 4.1. $^{15}\text{C}$

In Fig. 5, density profiles of  $^{15}\text{C}$  obtained from DRHBc calculations with PK1 are presented. The density distributions of protons and neutrons are shown in the left and right parts of Fig. 5(a), respectively. It is obvious that the neutron density extends much farther than protons, hinting a neutron halo in  $^{15}\text{C}$ .

As Fig. 4 shows, the valence neutron of  $^{15}\text{C}$  occupies the weakly bound level  $1/2_2^+$  with the occupation probability of 0.5. That is, the ground state spin-parity  $J^\pi = 1/2^+$ , which is consistent with experimental results as shown in Table 2. The main spherical components of the orbital  $1/2_2^+$  are  $1d_{5/2}$  and  $2s_{1/2}$  with probability amplitudes of 0.31 and 0.18. We define the probability amplitude of a spherical component in a deformed orbital as the product of the occupation probability of the orbital and the amplitude of the spherical component in the deformed wave function. The *s*-wave component of the weakly bound level  $1/2_2^+$  leads to the neutron halo in  $^{15}\text{C}$ .

The evolution of single neutron levels with deformation is studied by making constraint calculations. The SPLs of  $^{16}\text{C}$ , shown in Fig. 3, are used to guide us to determine the blocked level as a function of  $\beta_2$  in constraint calculations of  $^{15}\text{C}$ . The orbital  $5/2_1^+$  crosses  $1/2_2^+$  at  $\beta_2 \approx -0.06$  in SPLs of  $^{16}\text{C}$ . In the constraint calculations for  $^{15}\text{C}$ , the  $1/2_2^+$  level is blocked when  $\beta_2 \geq 0$  and each of the  $5/2_1^+$  and  $1/2_2^+$  orbitals is blocked respectively when  $\beta_2 < 0$  in order to get the SPLs corresponding to the lowest energy state. Thus obtained SPLs of  $^{15}\text{C}$  are shown in Fig. 6. It is found that there is a crossing between  $5/2_1^+$  and  $1/2_2^+$  at  $\beta_2 \approx -0.15$  in Fig. 6. This means

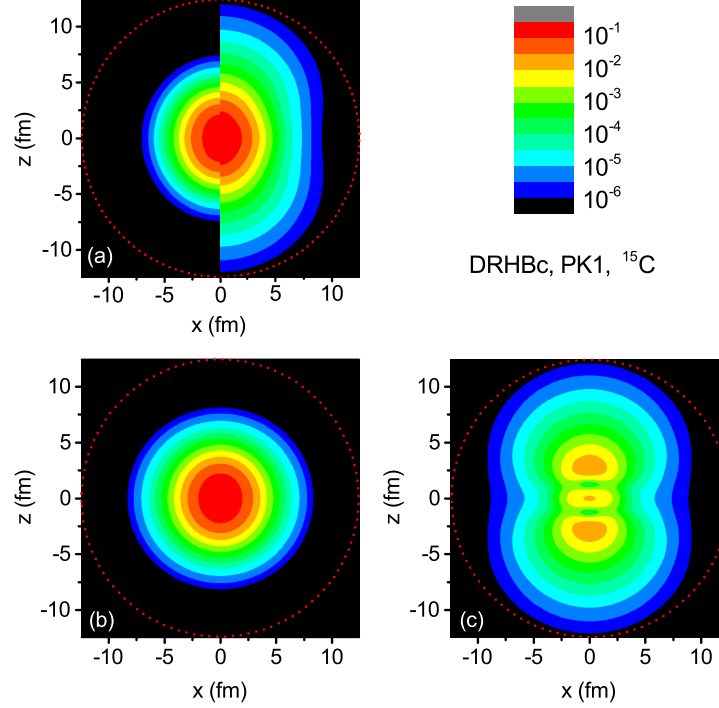


Figure 5: (Color online) Density profiles of  $^{15}\text{C}$  from DRHBc calculations with PK1. The  $z$ -axis is the symmetry axis. (a) The proton ( $x < 0$ ) and neutron ( $x > 0$ ) density profiles, (b) the density profile of the neutron core, and (c) the density profile of the neutron halo. In each plot, a dotted circle is drawn to guide the eye.

the valence orbital of neutron is  $1/2_2^+$  when  $\beta_2 > -0.15$  and  $5/2_1^+$  when  $\beta_2 < -0.15$ .

It is very interesting to see that in the spherical limit  $\beta_2 = 0$ , the neutron orbital  $\nu 2s_{1/2}$  is closer to  $\nu 1p_{1/2}$  than  $\nu 1d_{5/2}$ , i.e., the inversion of  $\nu 2s_{1/2}$  and  $\nu 1d_{5/2}$  appears in DRHBc calculations with PK1. This inversion plays a role for the formation of the one-neutron halo in  $^{15}\text{C}$ , which is similar to the case in  $^{11}\text{Li}$  [80, 115–117]. In the spherical limit, the valence neutron occupies an  $s$ -wave orbital, resulting in a pure  $s$ -wave halo in  $^{15}\text{C}$ . However, strong quadrupole correlations drive  $^{15}\text{C}$  to be prolate with  $\beta_2 = 0.26$  in the ground state and mix  $sd$  orbitals. The probability amplitude of  $s$ -wave component in the level  $1/2_2^+$  is about 0.18 in the ground state, which is smaller than the one in the spherical case with the value of 0.5. Furthermore, the  $1/2_2^+$  level is



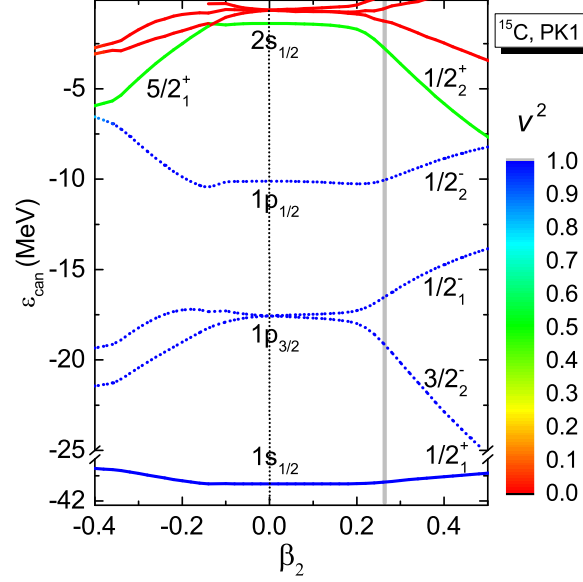


Figure 6: (Color online) Single neutron levels in the canonical basis of  $^{15}\text{C}$  from deformation constraint DRHBc calculations with PK1. When  $\beta_2 \neq 0$ , each level is labeled with  $\Omega_i^\pi$  where  $\pi$  is the parity,  $\Omega$  is the projection of the angular momentum on the symmetry axis, and  $i$  is used to order the level in each  $\Omega^\pi$ -block. The occupation probability  $\nu^2$  of each orbital is represented with different colors. The ground state is indicated by the gray vertical line.

more bound in the ground state compared with  $\nu 2s_{1/2}$  in the spherical limit. This means the deformation effects suppress the halo in  $^{15}\text{C}$ .

There is a big gap between the level  $1/2_2^+$  and  $1/2_2^-$  in the ground state of  $^{15}\text{C}$ , as seen in both Fig. 4 and Fig. 6. This gap is used to divide the total neutron density into the core and halo parts. The halo part comes from the weakly bound level  $1/2_2^+$  while the orbital  $1/2_2^-$  and those below are deeply bound and contribute to the core part. Density profiles of the core and the halo are presented in Fig. 5(b) and Fig. 5(c), respectively. It is obvious that the core of  $^{15}\text{C}$  shows a nearly spherical shape while the halo is prolate. This indicates the shape decoupling between the core and halo. Thus, the shape decoupling between the halo and core is predicted not only in even-even nuclei with a two-neutron halo [58–60], but also in odd  $A$  nuclei with a one-neutron halo.

In Fig. 7 the densities of the core and halo of  $^{15}\text{C}$  are respectively

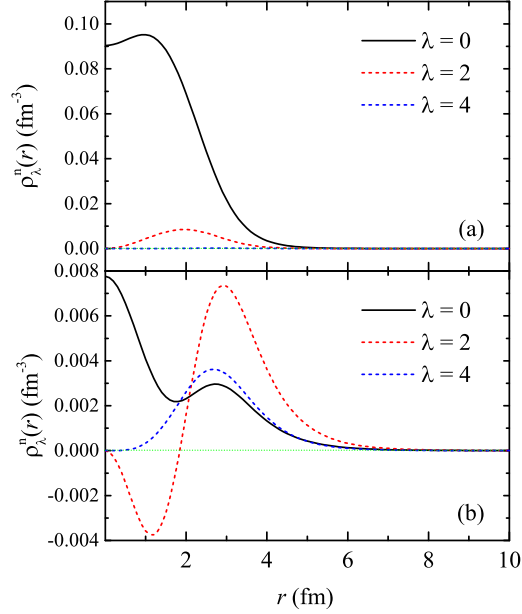


Figure 7: (Color online) The neutron density of  $^{15}\text{C}$  from DRHBc calculations with PK1 decomposed into spherical ( $\lambda = 0$ ), quadrupole ( $\lambda = 2$ ), and hexadecapole ( $\lambda = 4$ ) components for (a) the core and (b) the halo.

decomposed into spherical ( $\lambda = 0$ ), quadrupole ( $\lambda = 2$ ), and hexadecapole ( $\lambda = 4$ ) components [cf. Eq. (5)]. In Fig. 7(a), it can be found that the quadrupole component of the core is always positive with very small values compared with the spherical component, which corresponds to the nearly spherical (slightly prolate) core of  $^{15}\text{C}$  as shown in Fig. 5(b). The nearly spherical core of  $^{15}\text{C}$  is consistent with the spherical shape of  $^{14}\text{C}$  in Fig. 2. The quadrupole component of the halo density is mostly positive in Fig. 7(b). This agrees with the prolate shape of the density distribution of the halo shown in Fig. 5(c). The shape of the halo originates from the intrinsic structure of the  $1/2_2^+$  level. The angular distribution of the  $s$ -wave component is spherical; the angular distribution of the  $1d_{5/2}$  component in the level  $1/2_2^+$  is the mixing of  $|Y_{20}(\Omega)|^2$  and  $|Y_{21}(\Omega)|^2$  and it turns out that  $|Y_{20}(\Omega)|^2$  has a bigger amplitude. This means the halo density distribution is prolate because  $|Y_{20}(\Omega)|^2 \propto \cos^4 \theta$  [118].

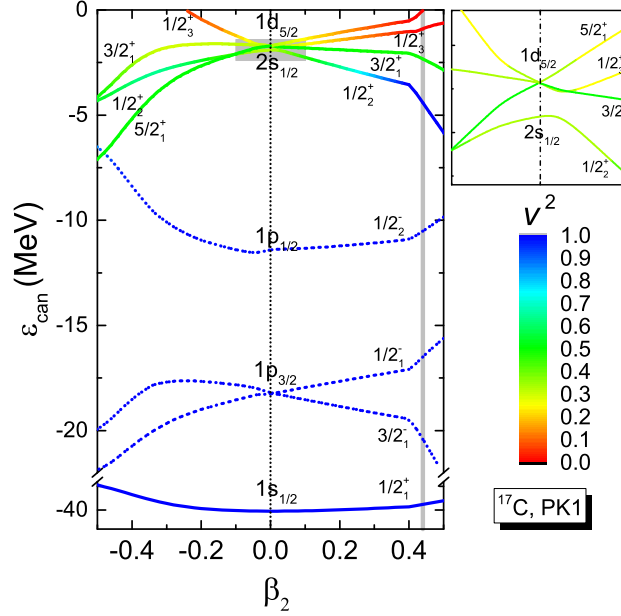


Figure 8: (Color online) Single neutron levels in the canonical basis of  $^{17}\text{C}$  from deformation constraint DRHBc calculations with PK1. When  $\beta_2 \neq 0$ , each level is labeled with  $\Omega_i^\pi$  where  $\pi$  is the parity,  $\Omega$  is the projection of the angular momentum on the symmetry axis, and  $i$  is used to order the level in each  $\Omega^\pi$ -block. The occupation probability  $\nu^2$  of each orbital is represented with different colors. The ground state is indicated by the gray vertical line. The shaded region with  $-0.1 \leq \beta_2 \leq 0.1$  and  $-2.3 \text{ MeV} \leq \epsilon_{\text{can}} \leq -1.3 \text{ MeV}$  is enlarged and shown on the right side.

#### 4.2. $^{17}\text{C}$

The single neutron levels of  $^{17}\text{C}$  in the ground state are shown in Fig. 4. The deformation parameter of the ground state is  $\beta_2 = 0.46$ . The valence neutron occupies the  $3/2_1^+$  orbital with the occupation probability of 0.5. The main spherical components of  $3/2_1^+$  are  $1d_{3/2}$  and  $1d_{5/2}$ . The ground state spin-parity from DRHBc calculations agrees with experiments [95, 104, 105]. There is no  $s$ -wave component in the valence orbital and  $^{17}\text{C}$  is not a halo nucleus in its ground state, which is contrary to the result from the SRHFB model [47]. Note that the halo structure may appear in low lying excited states of  $^{17}\text{C}$ , which has been investigated by using the halo effective field theory [119].

Deformation constraint calculations are performed for this nucleus and possible blocked levels can be singled out from the SPLs of  $^{18}\text{C}$  shown in

Fig. 3. The constraint calculation of  $^{17}\text{C}$  is more complex compared with  $^{15}\text{C}$ , because the level density around  $\epsilon_{\text{can}} \approx -2$  MeV is higher and there are several crossings among single neutron levels. The SPLs of  $^{17}\text{C}$  are shown in Fig. 8. Note that for an odd- $A$  nucleus, the bulk properties depend on which orbital is blocked [120]; so do SPLs in self-consistent calculations. Therefore one can get several sets of SPLs when various orbitals around the neutron Fermi surface is blocked. When getting SPLs shown in Fig. 8, the orbital  $3/2_1^+$  is blocked for the region  $\beta_2 > 0$  and  $5/2_1^+$  is blocked when  $\beta_2 < 0$ . Since both orbitals are from  $\nu 1d_{5/2}$ , the SPLs are continuous at  $\beta_2 = 0$ . There is a sudden change in the slope of each single neutron level at  $\beta_2 \approx 0.40$  where the pairing energy diminishes to zero. From the enlarged figure shown on the right side of Fig. 8, one can notice that the neutron orbital  $\nu 2s_{1/2}$  is lower than  $\nu 1d_{5/2}$  in the spherical limit in  $^{17}\text{C}$  with PK1.

#### 4.3. $^{19}\text{C}$

The intrinsic shape of the ground state of  $^{19}\text{C}$  is oblate with  $\beta_2 = -0.45$  and the rms matter radius is 3.02 fm in DRHBc calculations with PK1. The valence orbital is the weakly bound level  $3/2_1^+$  with the occupation probability of 0.5. The main spherical components of the  $3/2_1^+$  level are  $d$ -waves. So the ground state of  $^{19}\text{C}$  does not show a halo structure. This is contrary to the experimental results [95, 104, 106, 107]. The SPLs in the ground state of  $^{19}\text{C}$  are shown in Fig. 4. Quadrupole deformation constraint calculations for  $^{19}\text{C}$  are carried out and the evolution of SPLs with  $\beta_2$  is given in Fig. 9. From the single neutron spectrum of  $^{19}\text{C}$  shown in Fig. 9, one can conclude that the valence neutron occupies the  $3/2_1^+$  orbital when  $\beta_2 < 0$  and the  $1/2_3^+$  orbital when  $\beta_2 > 0$ . It is seen that the inversion of  $(\nu 2s_{1/2}, \nu 1d_{5/2})$  in the spherical limit also exists in  $^{19}\text{C}$  with PK1.

Many theoretical studies support an  $s$ -wave halo in  $^{19}\text{C}$  [47, 121–125]. The ground state spin-parity of  $^{19}\text{C}$  is confirmed to be  $J^\pi = 1/2^+$  [95, 104, 106, 107, 126], implying a prolate intrinsic deformation [126, 127]. Recently  $^{19}\text{C}$  is investigated by using the complex momentum representation method [128] and the authors reproduced the halo structure in  $^{19}\text{C}$  with the last valence neutron occupying the  $1/2^+$  orbital and the quadrupole deformation  $0.2 < \beta_2 < 0.4$ . In DRHBc calculations with PK1, there is a second energy minimum ( $E^* = 1.57$  MeV) in the potential energy surface when the neutron level  $1/2_3^+$  is blocked. The  $\beta_2$  value corresponding to this energy minimum is 0.37 which is very close to the one obtained from deformed Skyrme HF calculations with SGII [53]. Single neutron levels corresponding

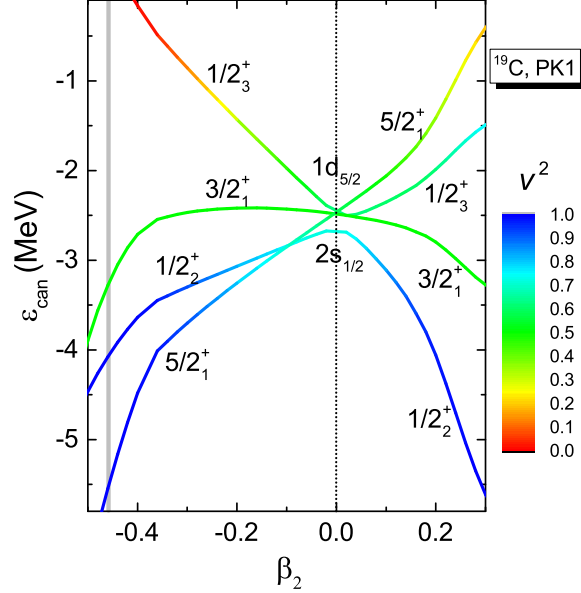


Figure 9: (Color online) Single neutron levels in the  $sd$  shell in the canonical basis of  $^{19}\text{C}$  from deformation constraint DRHBc calculations with PK1. When  $\beta_2 \neq 0$ , each level is labeled with  $\Omega_i^\pi$  where  $\pi$  is the parity,  $\Omega$  is the projection of the angular momentum on the symmetry axis, and  $i$  is used to order the level in each  $\Omega^\pi$ -block. The occupation probability  $\nu^2$  of each orbital is represented with different colors. The ground state is indicated by the gray vertical line.

to this local energy minimum are given in Fig. 4, labeled as  $^{19}\text{C}^*$ . The one-neutron separation energy of  $^{19}\text{C}^*$  is 0.03 MeV. With a so small one-neutron separation energy,  $^{19}\text{C}^*$  can be regarded as a  $^{18}\text{C}+n$  system. The valance orbital is the  $1/2_3^+$  level, of which the main spherical components are  $2s_{1/2}$  and  $1d_{5/2}$  with probability amplitudes of 0.33 and 0.15. The halo is thus formed in  $^{19}\text{C}^*$ , as the result of the appearance of the  $s$ -wave component in the valance orbital  $1/2_3^+$ .

Due to the inversion of  $(\nu 2s_{1/2}, \nu 1d_{5/2})$ , the valance neutron occupies  $d$ -wave orbital and no halo appears in the spherical limit. When  $\beta_2 > 0$ , the level  $\nu 1d_{5/2}$  splits into three. For the highest,  $5/2_1^+$ , and the lowest,  $3/2_1^+$ , the main components are both  $\nu 1d_{5/2}$ . Strong quadrupole correlations mix the  $sd$  orbitals and lead to the appearance of an  $s$ -wave component in the valance orbital  $1/2_3^+$ . Thus, deformation effects are favorable to the formation of the one-neutron halo in  $^{19}\text{C}^*$  under the inversion of  $(\nu 2s_{1/2}, \nu 1d_{5/2})$ .

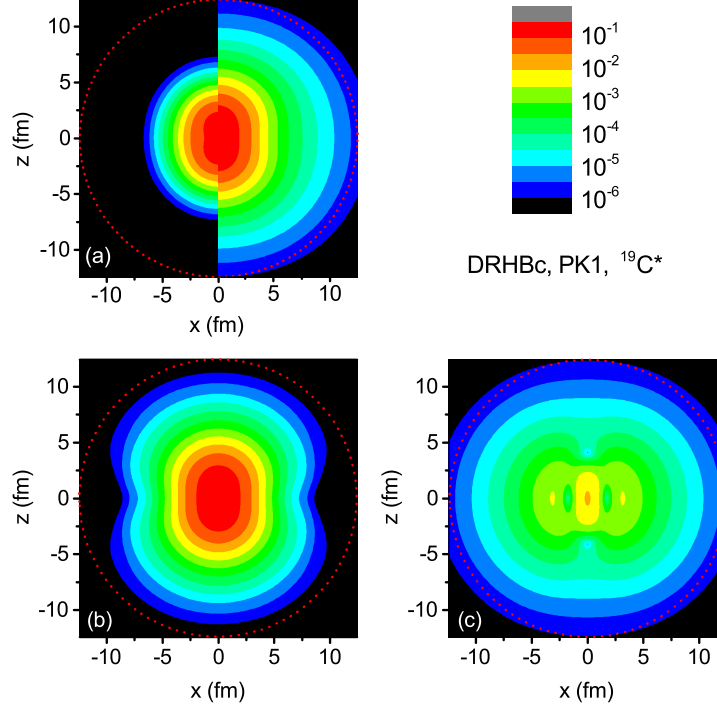


Figure 10: (Color online) Density profiles of  $^{19}\text{C}^*$  from DRHBc calculations with PK1. The  $z$ -axis is the symmetry axis. (a) The proton ( $x < 0$ ) and neutron ( $x > 0$ ) density profiles, (b) the density profile of the neutron core, and (c) the density profile of the neutron halo. In each plot, a dotted circle is drawn to guide the eye.

Proton and neutron density profiles for  $^{19}\text{C}^*$  are given in Fig. 10(a). The total neutron density is divided into the core and halo parts. The halo part comes from the weakly bound and valence orbital  $1/2_3^+$ . The orbital  $3/2_1^+$  and those below are deeply bound and contribute to the core. Density profiles of the core and halo are presented in Fig. 10(b) and Fig. 10(c), respectively. The neutron halo is hinted by the large extension of the neutron density. It can be seen that the core of  $^{19}\text{C}^*$  shows a prolate shape while the halo density distribution is slightly oblate.

Spherical ( $\lambda = 0$ ), quadrupole ( $\lambda = 2$ ), and hexadecapole ( $\lambda = 4$ ) components [cf. Eq. (5)] of the core and halo density are shown in Figs. 11(a) and (b). The quadrupole component of the core density is always positive which is consistent with the prolate shape of the core density distribution

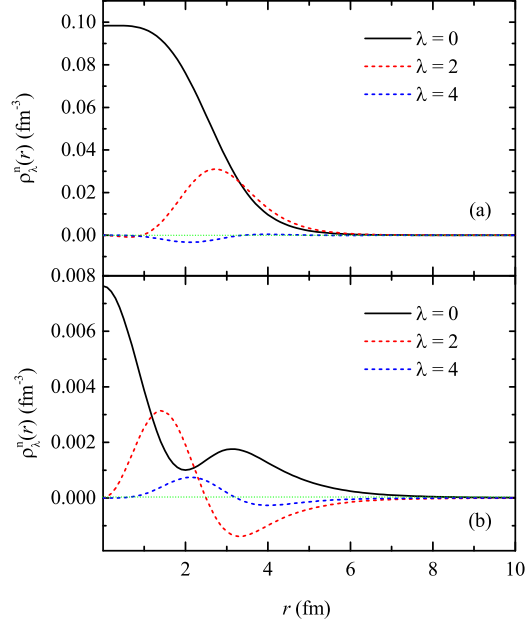


Figure 11: (Color online) The neutron density of  $^{19}\text{C}^*$  from DRHBc calculations with PK1 decomposed into spherical ( $\lambda = 0$ ), quadrupole ( $\lambda = 2$ ), and hexadecapole ( $\lambda = 4$ ) components for (a) the core and (b) the halo.

presented in Fig. 10(b). The quadrupole component of the halo density is positive when  $r < 2.5$  fm and negative when  $r > 2.5$  fm. Although it looks that the positive amplitude dominates, the quadrupole moment of the halo part is actually negative due to the factor  $r^2$  in  $Q_2 \propto \langle r^2 P_2(\cos\theta) \rangle$ . This indicates an oblate shape of the halo and the shape decoupling between the core and halo appears in  $^{19}\text{C}^*$ .

Up to now, we have discussed the structure of  $^{15,17}\text{C}$  and  $^{19}\text{C}$  in detail. We emphasize that the inversion of  $(\nu 2s_{1/2}, \nu 1d_{5/2})$  together with quadrupole correlations determine the configuration of the valence neutron orbital in these three odd  $A$  nuclei. The occupation and closeness to the threshold of the second and third  $1/2^+$  levels, originating from  $\nu 2s_{1/2}$  or  $\nu 1d_{5/2}$ , determine whether or not a halo may appear. We should also stress that the halo in the ground state of  $^{19}\text{C}$  is not reproduced in our DRHBc calculations with PK1, though a deformed halo appears in the second minimum of the potential energy curve with  $1/2_3^+$  blocked. This problem should be addressed in future investigations.

## 5. Halo in $^{22}\text{C}$

It is believed that the halo in  $^{22}\text{C}$  is caused by  $s$ -wave valence neutrons [3, 4, 13, 21, 30, 47, 129–148], but the probability amplitude of the  $s$ -wave component is still not well determined. In Ref. [58], the DRHBc theory has been used to study  $^{22}\text{C}$  and it was revealed that the probability amplitude of the  $s$ -wave component is about 0.25. This value is connected with quadrupole correlations and the shell evolution characterized by the inversion of  $(\nu 2s_{1/2}, \nu 1d_{5/2})$ . This inversion has been predicted in  $A/Z \sim 3$  nuclei [23] and the appearance of shell closures at  $N = 14$  and  $N = 16$  is closely related to the competition between  $\nu 2s_{1/2}$  and  $\nu 1d_{5/2}$  [18, 22–29, 31].

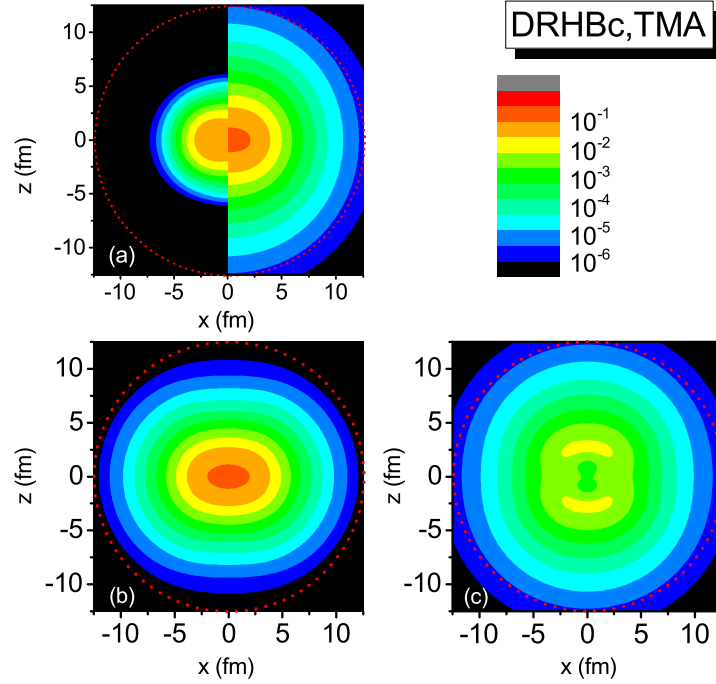


Figure 12: (Color online) Density profiles of  $^{22}\text{C}$  from DRHBc calculations with TMA. The  $z$ -axis is the symmetry axis. (a) The proton ( $x < 0$ ) and neutron ( $x > 0$ ) density profiles, (b) the density profile of the neutron core, and (c) the density profile of the neutron halo. In each plot, a dotted circle is drawn to guide the eye.

In Ref. [58], DRHBc calculations were made with the effective interaction PK1. To investigate the parameter dependence and learn more about the results from the DRHBc theory, we have carried out calculations with



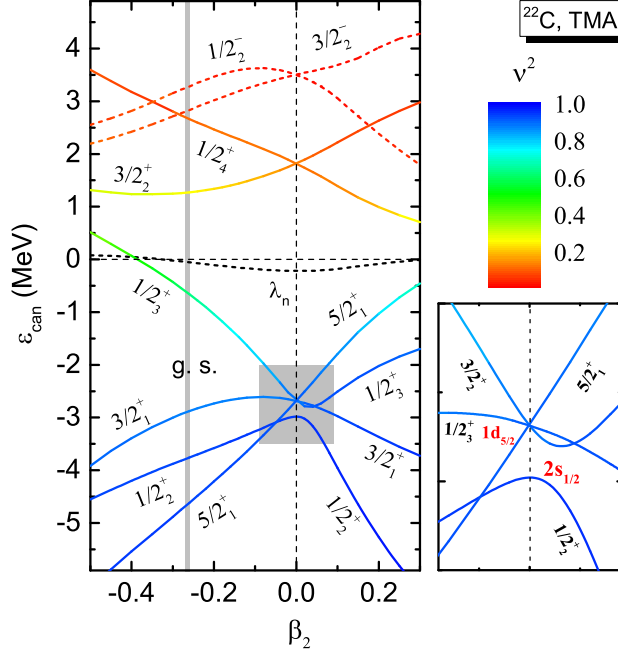


Figure 13: (Color online) Single neutron levels around the Fermi level in the canonical basis of  $^{22}\text{C}$  from deformation constraint DRHBc calculations with TMA. Each level is labeled with  $\Omega_i^\pi$  where  $\pi$  is the parity,  $\Omega$  is the projection of the angular momentum on the symmetry axis, and  $i$  is used to order the level in each  $\Omega^\pi$ -block. The Fermi level ( $\lambda_n$ ) is displayed by the black dashed line. The occupation probability  $\nu^2$  of each orbital is represented with different colors. The ground state is indicated by the gray vertical line. The shaded region with  $-0.1 \leq \beta_2 \leq 0.1$  and  $-3.2 \text{ MeV} \leq \epsilon_{\text{can}} \leq -2.0 \text{ MeV}$  is enlarged and shown on the right side.

effective interactions NL3 and TMA. As mentioned earlier, with NL3 the Borromean feature of  $^{22}\text{C}$  cannot be reproduced. Next we present the DRHBc results for  $^{22}\text{C}$  with the parameter set TMA [149]. The strength of the pairing force  $V_0$  is taken as  $400 \text{ MeV fm}^3$ . Other parameters are the same as those mentioned in Sec. 3. The calculated one-neutron separation energy of  $^{21}\text{C}$  is  $-0.56 \text{ MeV}$  and two-neutron separation energy of  $^{22}\text{C}$  is  $0.65 \text{ MeV}$ ; i.e.,  $^{22}\text{C}$  is a Borromean nucleus. Considering the large uncertainties in  $S_{2n}$  of  $^{22}\text{C}$ , it should be expected that when  $V_0$  is within a range containing this specific value, the Borromean feature of  $^{22}\text{C}$  can also be reproduced. The ground state of  $^{22}\text{C}$  has an oblate intrinsic deformation with  $\beta_2 = -0.27$ , which is similar to the result with PK1. The calculated rms matter radius  $R_m$  of  $^{22}\text{C}$

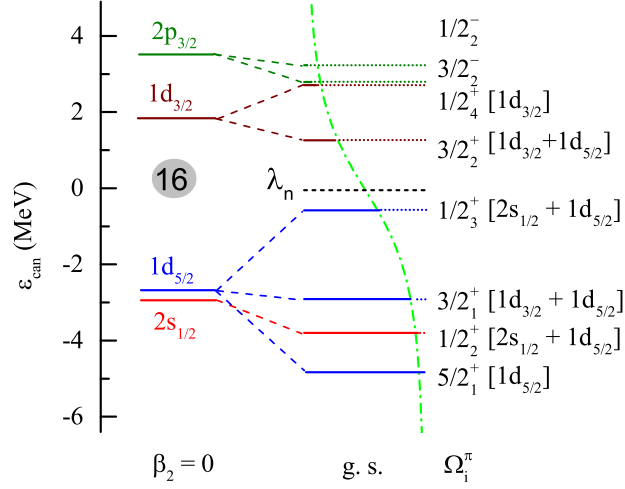


Figure 14: (Color online) Single neutron orbitals around the Fermi level ( $\lambda_n$ ) of  $^{22}\text{C}$  in the canonical basis in the spherical limit and at the ground state (g.s.) obtained from DRHBc calculations with TMA. For the case of the ground state, the length of the solid line is proportional to the occupation probability of each level calculated from the DRHBc theory. The dash-dotted line corresponds to the occupation probability calculated from the BCS formula with an average pairing gap. Quantum numbers  $\Omega_i^\pi$  and the main Woods-Saxon components are given for orbitals in the  $sd$  shell.

is 3.39 fm with TMA. This value is consistent with the data  $3.44 \pm 0.08$  fm [4] and  $3.38 \pm 0.10$  fm [13] but much smaller than the datum  $5.4 \pm 0.9$  fm [3].

Next we discuss density profiles (Fig. 12), single neutron levels as a function of  $\beta_2$  (Fig. 13), single neutron levels corresponding to the ground state and the spherical shape (Fig. 14), and different components of the halo and core densities (Fig. 15) for  $^{22}\text{C}$ . It will be seen that these results from DRHBc calculations with TMA are similar to those with PK1 [58].

The neutron halo in  $^{22}\text{C}$  with TMA can be clearly seen in Fig. 12(a). In the single neutron spectrum of  $^{22}\text{C}$  with TMA shown in Fig. 13 and Fig. 14, there is a big gap between the two orbitals  $1/2_3^+$  and  $3/2_1^+$ . Taking advantage of this gap, the total neutron density is decomposed into the core and halo parts. The level  $3/2_1^+$  and those below it contribute to the core. The halo part comes from the level  $1/2_3^+$  and those above it. The neutron density distributions of the core and halo are shown in Figs. 12(b) and (c). The density distribution of the halo (core) shows a (an) prolate (oblate) shape. This means the shape decoupling of the core and halo is predicted

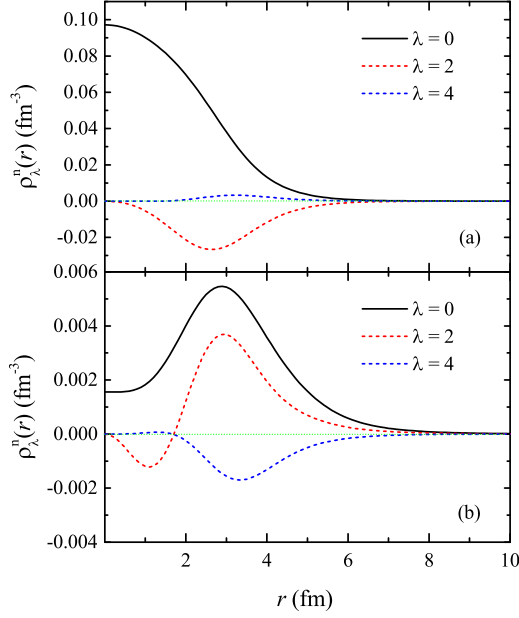


Figure 15: (Color online) The neutron density of  $^{22}\text{C}$  from DRHBc calculations with PK1 decomposed into spherical ( $\lambda = 0$ ), quadrupole ( $\lambda = 2$ ), and hexadecapole ( $\lambda = 4$ ) components for (a) the core and (b) the halo.

in calculations with both PK1 and TMA. Different components of the core and halo density distributions are presented in Figs. 15(a) and (b). The quadrupole components of the core and halo density, represented by red dashed line, are smaller than zero and mostly positive, respectively, being consistent with shapes of density profiles given in Figs. 12(b) and (c).

The inversion of  $\nu 2s_{1/2}$  and  $\nu 1d_{5/2}$  is also found in DRHBc calculations with TMA and the shell evolution with deformation is similar to that calculated with PK1. The shell closure at  $N = 16$  can be seen in the spherical limit but disappears at the deformed ground state. Recently, shell model calculations of  $^{22}\text{C}$  and  $^{24}\text{O}$  with continuum considered [150] also predicted a halo in  $^{22}\text{C}$ . The calculated energy of the first excited state for  $^{22}\text{C}$  is much smaller than the one in  $^{24}\text{O}$ , hinting the disappearance of the shell closure at  $N = 16$  in  $^{22}\text{C}$ .

## 6. Summary

In this work, ground state properties of carbon isotopes are studied in detail by using the DRHBc theory and compared with experiments. The DRHBc calculations with the effective interaction PK1 can give a reasonably good description for bulk properties of nuclei in this isotopic chain. These carbon isotopes exhibit a variety of intrinsic shapes, changing abruptly with the neutron number: spherical  $^{13,14}\text{C}$ , prolate  $^{15,17}\text{C}$ , and oblate  $^{12,16,18,19,20,22}\text{C}$ . Deformation constraint calculations are performed in order to examine the evolution of SPLs with  $\beta_2$ . When  $^{15-20,22}\text{C}$  are constrained to be spherical, the two neutron orbitals  $\nu 1d_{5/2}$  and  $\nu 2s_{1/2}$  are nearly degenerate but inverted compared with the order of single neutron orbitals in stable nuclei, leading to the appearance of a shell closure at  $N = 16$ . When considering deformation effects, these nuclei are all deformed and the shell closure at  $N = 16$  disappears.

We have investigated halo structures in  $^{15,19,22}\text{C}$ . In these three nuclei, halo configurations are closely associated with the inversion of  $(\nu 2s_{1/2}, \nu 1d_{5/2})$ , deformation effects, and the shell evolution. Halos in these nuclei are all caused by a  $s$ -wave component in wave functions of valence neutron(s).  $^{15}\text{C}$  is a one-neutron halo and the intrinsic shape of its ground is prolate with  $\beta_2 = 0.26$ . The inversion of  $(\nu 2s_{1/2}, \nu 1d_{5/2})$  leads to the formation of the halo because, when constrained to be spherical, the weakly bound orbital  $\nu 2s_{1/2}$  is occupied by the valence neutron. However, the deformation effects suppress the halo in  $^{15}\text{C}$  due to the following two interwoven reasons: (i) the valence orbital is  $1/2_2^+$  which is more bound than  $\nu 2s_{1/2}$  (in the spherical limit); (ii) the level  $1/2_2^+$  is a mixture mainly of  $\nu 2s_{1/2}$  and  $\nu 1d_{5/2}$  and not purely of  $s$ -wave. It is well accepted that  $^{19}\text{C}$  is a halo nucleus in its ground state with  $J^\pi = 1/2^+$ . The ground state of  $^{19}\text{C}$  in DRHBc calculations with PK1 shows an oblate shape with the spin-parity of  $3/2^+$  and does not have a halo structure. Nevertheless, an isomeric state  $^{19}\text{C}^*$  with  $\beta_2 = 0.37$  corresponding to the second energy minimum of the potential energy surface with the third  $1/2^+$  neutron level blocked does show an  $s$ -wave halo. It should be further investigated why our DRHBc results for  $^{19}\text{C}$  is at odds with the experiment.  $^{22}\text{C}$  is reexamined with TMA and similar results have been obtained as those presented in Ref. [58] with PK1.

For  $^{19}\text{C}$  and  $^{22}\text{C}$ , in the spherical limit, the valence orbital is  $\nu 1d_{5/2}$  and no halo can be formed. Quadrupole correlations mix  $sd$  waves and lead to the appearance of non-negligible  $s$ -wave components in the weakly bound

orbital  $1/2_3^+$  which is the only valence orbital in  $^{19}\text{C}^*$  and the most dominant one in  $^{22}\text{C}$ . This means deformation effects are conducive to the formation of halos in  $^{19}\text{C}^*$  and  $^{22}\text{C}$ .

We have shown shape decoupling effects in  $^{15}\text{C}$ ,  $^{19}\text{C}^*$ , and  $^{22}\text{C}$  with a nearly spherical core but a prolate halo, a prolate core but a slightly oblate halo, and an oblate core but a prolate halo, respectively. We conclude that the shape decoupling between the halo and core exists not only in even-even nuclei but also in odd  $A$  nuclei.

## Acknowledgements

We thank the DRHBc Mass Table Collaboration, Yu-Ting Rong, and Kun Wang for helpful discussions. This work has been supported by the National Key R&D Program of China (Grant No. 2018YFA0404402), the National Natural Science Foundation of China (Grants No. 11525524, No. 11621131001, No. 11947302, and No. 11961141004), the Key Research Program of Frontier Sciences of Chinese Academy of Sciences (No. QYZDB-SSWSYS013), the Strategic Priority Research Program of Chinese Academy of Sciences (Grant No. XDB34010000), the Inter-Governmental S&T Cooperation Project between China and Croatia, and the IAEA Coordinated Research Project “F41033”. The results described in this paper are obtained on the High-performance Computing Cluster of ITP-CAS and the ScGrid of the Supercomputing Center, Computer Network Information Center of Chinese Academy of Sciences.

## References

- [1] D. Bazin, W. Benenson, B. A. Brown, J. Brown, B. Davids, M. Fauerbach, P. G. Hansen, P. Mantica, D. J. Morrissey, C. F. Powell, B. M. Sherrill, M. Steiner, [Probing the halo structure of  \$^{19,17,15}\text{C}\$  and  \$^{14}\text{B}\$](#) , Phys. Rev. C 57 (1998) 2156–2164.
- [2] D. Q. Fang, T. Yamaguchi, T. Zheng, A. Ozawa, M. Chiba, R. Kanungo, T. Kato, K. Morimoto, T. Ohnishi, T. Suda, Y. Yamaguchi, A. Yoshida, K. Yoshida, I. Tanihata, [One-neutron halo structure in  \$^{15}\text{C}\$](#) , Phys. Rev. C 69 (2004) 034613.
- [3] K. Tanaka, T. Yamaguchi, T. Suzuki, T. Ohtsubo, M. Fukuda, D. Nishimura, M. Takechi, K. Ogata, A. Ozawa, T. Izumikawa,

- T. Aiba, N. Aoi, H. Baba, Y. Hashizume, K. Inafuku, N. Iwasa, K. Kobayashi, M. Komuro, Y. Kondo, T. Kubo, M. Kurokawa, T. Matsuyama, S. Michimasa, T. Motobayashi, T. Nakabayashi, S. Nakajima, T. Nakamura, H. Sakurai, R. Shinoda, M. Shinohara, H. Suzuki, E. Takeshita, S. Takeuchi, Y. Togano, K. Yamada, T. Yasuno, M. Yoshitake, [Observation of a large reaction cross section in the drip-line nucleus  \$^{22}\text{C}\$](#) , Phys. Rev. Lett. 104 (2010) 062701.
- [4] Y. Togano, T. Nakamura, Y. Kondo, J. Tostevin, A. Saito, J. Gibelin, N. Orr, N. Achouri, T. Aumann, H. Baba, F. Delaunay, P. Doornenbal, N. Fukuda, J. Hwang, N. Inabe, T. Isobe, D. Kameda, D. Kanno, S. Kim, N. Kobayashi, T. Kobayashi, T. Kubo, S. Leblond, J. Lee, F. Marques, R. Minakata, T. Motobayashi, D. Murai, T. Murakami, K. Muto, T. Nakashima, N. Nakatsuka, A. Navin, S. Nishi, S. Ogoshi, H. Otsu, H. Sato, Y. Satou, Y. Shimizu, H. Suzuki, K. Takahashi, H. Takeda, S. Takeuchi, R. Tanaka, A. Tuff, M. Vandebrouck, K. Yoneda, [Interaction cross section study of the two-neutron halo nucleus  \$^{22}\text{C}\$](#) , Phys. Lett. B 761 (2016) 412–418.
- [5] G. Audi, F. G. Kondev, M. Wang, W. Huang, S. Naimi, [The NUBASE2016 evaluation of nuclear properties](#), Chin. Phys. C. 41 (3) (2017) 030001.
- [6] W. J. Huang, G. Audi, M. Wang, F. G. Kondev, S. Naimi, X. Xu, [The AME2016 atomic mass evaluation \(I\). Evaluation of input data; and adjustment procedures](#), Chin. Phys. C. 41 (3) (2017) 030002.
- [7] M. Wang, G. Audi, F. Kondev, W. Huang, S. Naimi, X. Xu, [The AME2016 atomic mass evaluation \(II\). tables, graphs and references](#), Chin. Phys. C 41 (3) (2017) 030003.
- [8] L. Gaudefroy, W. Mittig, N. A. Orr, S. Varet, M. Chartier, P. Roussel-Chomaz, J. P. Ebran, B. Fernández-Domínguez, G. Frémont, P. Gangnant, A. Gillibert, S. Grévy, J. F. Libin, V. A. Maslov, S. Paschalis, B. Pietras, Y.-E. Penionzhkevich, C. Spitaels, A. C. C. Villari, [Direct mass measurements of  \$^{19}\text{B}\$ ,  \$^{22}\text{C}\$ ,  \$^{29}\text{F}\$ ,  \$^{31}\text{Ne}\$ ,  \$^{34}\text{Na}\$  and other light exotic nuclei](#), Phys. Rev. Lett. 109 (2012) 202503.
- [9] G. Audi, F. G. Kondev, M. Wang, B. Pfeiffer, X. Sun, J. Blachot,

- M. MacCormick, [The NUBASE2012 evaluation of nuclear properties](#), Chin. Phys. C 36 (12) (2012) 1157–1286.
- [10] G. Audi, M. Wang, A. H. Wapstra, F. G. Kondev, M. MacCormick, X. Xu, B. Pfeiffer, [The NUBASE2012 evaluation of nuclear properties \(I\). Evaluation of input data, adjustment procedures](#), Chin. Phys. C 36 (12) (2012) 1287–1602.
- [11] M. Wang, G. Audi, A. H. Wapstra, F. G. Kondev, M. MacCormick, X. Xu, B. Pfeiffer, [The NUBASE2012 evaluation of nuclear properties \(II\). Tables, graphs and references](#), Chin. Phys. C 36 (12) (2012) 1603–2014.
- [12] R. Kanungo, W. Horiuchi, G. Hagen, G. R. Jansen, P. Navratil, F. Ameil, J. Atkinson, Y. Ayyad, D. Cortina-Gil, I. Dillmann, A. Estradé, A. Evdokimov, F. Farinon, H. Geissel, G. Guastalla, R. Janik, M. Kimura, R. Knöbel, J. Kurcewicz, Y. A. Litvinov, M. Marta, M. Mostazo, I. Mukha, C. Nociforo, H. J. Ong, S. Pietri, A. Prochazka, C. Scheidenberger, B. Sitar, P. Strmen, Y. Suzuki, M. Takechi, J. Tanaka, I. Tanihata, S. Terashima, J. Vargas, H. Weick, J. S. Winfield, [Proton distribution radii of  \$^{12-19}\text{C}\$  illuminate features of neutron halos](#), Phys. Rev. Lett. 117 (2016) 102501.
- [13] T. Nagahisa, W. Horiuchi, [Examination of the  \$^{22}\text{C}\$  radius determination with interaction cross sections](#), Phys. Rev. C 97 (2018) 054614.
- [14] I. Tanihata, H. Savajols, R. Kanungo, [Recent experimental progress in nuclear halo structure studies](#), Prog. Part. Nucl. Phys. 68 (2013) 215 – 313.
- [15] J. Dobaczewski, I. Hamamoto, W. Nazarewicz, J. A. Sheikh, [Nuclear shell structure at particle drip lines](#), Phys. Rev. Lett. 72 (1994) 981–984.
- [16] J. Meng, I. Tanihata, S. Yamaji, [The proton and neutron distributions in Na isotopes: The development of halo and shell structure](#), Phys. Lett. B 419 (1998) 1–6.

- [17] W. H. Long, P. Ring, J. Meng, N. Van Giai, C. A. Bertulani, [Nuclear halo structure and pseudospin symmetry](#), Phys. Rev. C 81 (2010) 031302.
- [18] T. Otsuka, A. Gade, O. Sorlin, T. Suzuki, Y. Utsuno, [Evolution of shell structure in exotic nuclei](#), Rev. Mod. Phys. 92 (2020) 015002.
- [19] D. T. Tran, H. J. Ong, G. Hagen, T. D. Morris, N. Aoi, T. Suzuki, Y. Kanada-En'yo, L. S. Geng, S. Terashima, I. Tanihata, T. T. Nguyen, Y. Ayyad, P. Y. Chan, M. Fukuda, H. Geissel, M. N. Harakeh, T. Hashimoto, T. H. Hoang, E. Ideguchi, A. Inoue, G. R. Jansen, R. Kanungo, T. Kawabata, L. H. Khiem, W. P. Lin, K. Matsuta, M. Mihara, S. Momota, D. Nagae, N. D. Nguyen, D. Nishimura, T. Otsuka, A. Ozawa, P. P. Ren, H. Sakaguchi, C. Scheidenberger, J. Tanaka, M. Takechi, R. Wada, T. Yamamoto, [Evidence for prevalent  \$Z = 6\$  magic number in neutron-rich carbon isotopes](#), Nat. Commun. 9 (1) (2018) 1594.
- [20] M. Stanoiu, D. Sohler, O. Sorlin, F. Azaiez, Z. Dombrádi, B. A. Brown, M. Bellegric, C. Borcea, C. Bourgeois, Z. Dlouhy, Z. Elekes, Z. Fülöp, S. Grévy, D. Guillemaud-Mueller, F. Ibrahim, A. Kerek, A. Krasznahorkay, M. Lewitowicz, S. M. Lukyanov, S. Mandal, J. Mrázek, F. Negoita, Y.-E. Penionzhkevich, Z. Podolyák, P. Roussel-Chomaz, M. G. Saint-Laurent, H. Savajols, G. Sletten, J. Timár, C. Timis, A. Yamamoto, [Disappearance of the  \$N = 14\$  shell gap in the carbon isotopic chain](#), Phys. Rev. C 78 (2008) 034315.
- [21] W. Horiuchi, Y. Suzuki,  [\$^{22}\text{C}\$ : An  \$s\$ -wave two-neutron halo nucleus](#), Phys. Rev. C 74 (2006) 034311.
- [22] O. Sorlin, M.-G. Porquet, [Nuclear magic numbers: New features far from stability](#), Prog. Part. Nucl. Phys. 61 (2) (2008) 602 – 673.
- [23] A. Ozawa, T. Kobayashi, T. Suzuki, K. Yoshida, I. Tanihata, [New magic number,  \$N = 16\$ , near the neutron drip line](#), Phys. Rev. Lett. 84 (2000) 5493–5495.
- [24] T. Otsuka, R. Fujimoto, Y. Utsuno, B. A. Brown, M. Honma, T. Mizusaki, [Magic numbers in exotic nuclei and spin-isospin properties of the  \$NN\$  interaction](#), Phys. Rev. Lett. 87 (2001) 082502.



- [25] D. Cortina-Gil, J. Fernandez-Vazquez, T. Aumann, T. Baumann, J. Benlliure, M. J. G. Borge, L. V. Chulkov, U. Datta Pramanik, C. Forssén, L. M. Fraile, H. Geissel, J. Gerl, F. Hammache, K. Itahashi, R. Janik, B. Jonson, S. Mandal, K. Markenroth, M. Meister, M. Mocko, G. Münzenberg, T. Ohtsubo, A. Ozawa, Y. Prezado, V. Pribora, K. Riisager, H. Scheit, R. Schneider, G. Schrieder, H. Simon, B. Sitar, A. Stolz, P. Strmen, K. Sümmerer, I. Szarka, H. Weick, [Shell structure of the near-dripline nucleus  \$^{23}\text{O}\$](#) , Phys. Rev. Lett. 93 (2004) 062501.
- [26] B. A. Brown, W. A. Richter, [Magic numbers in the neutron-rich oxygen isotopes](#), Phys. Rev. C 72 (2005) 057301.
- [27] E. Becheva, Y. Blumenfeld, E. Khan, D. Beaumel, J. M. Daugas, F. Delaunay, C.-E. Demonchy, A. Drouart, M. Fallot, A. Gillibert, L. Giot, M. Grasso, N. Keeley, K. W. Kemper, D. T. Khoa, V. Lapoux, V. Lima, A. Musumarra, L. Nalpas, E. C. Pollacco, O. Roig, P. Roussel-Chomaz, J. E. Sauvestre, J. A. Scarpaci, F. Skaza, H. S. Than, [N = 14 shell closure in  \$^{22}\text{O}\$  viewed through a neutron sensitive probe](#), Phys. Rev. Lett. 96 (2006) 012501.
- [28] R. Kanungo, C. Nociforo, A. Prochazka, T. Aumann, D. Boutin, D. Cortina-Gil, B. Davids, M. Diakaki, F. Farinon, H. Geissel, R. Gernhäuser, J. Gerl, R. Janik, B. Jonson, B. Kindler, R. Knöbel, R. Krücken, M. Lantz, H. Lenske, Y. Litvinov, B. Lommel, K. Mahata, P. Maierbeck, A. Musumarra, T. Nilsson, T. Otsuka, C. Perro, C. Scheidenberger, B. Sitar, P. Strmen, B. Sun, I. Szarka, I. Tanihata, Y. Utsuno, H. Weick, M. Winkler, [One-neutron removal measurement reveals  \$^{24}\text{O}\$  as a new doubly magic nucleus](#), Phys. Rev. Lett. 102 (2009) 152501.
- [29] C. Hoffman, T. Baumann, D. Bazin, J. Brown, G. Christian, D. Denby, P. DeYoung, J. Finck, N. Frank, J. Hinnefeld, S. Mosby, W. Peters, W. Rogers, A. Schiller, A. Spyrou, M. Scott, S. Tabor, M. Thoennessen, P. Voss, [Evidence for a doubly magic  \$^{24}\text{O}\$](#) , Phys. Lett. B 672 (1) (2009) 17–21.
- [30] L. Coraggio, A. Covello, A. Gargano, N. Itaco, [Shell-model calculations for neutron-rich carbon isotopes with a chiral nucleon-nucleon potential](#), Phys. Rev. C 81 (2010) 064303.

- [31] R. Kanungo, [A new view of nuclear shells](#), Phys. Scr. 2013 (T152) (2013) 014002.
- [32] A. Tohsaki, H. Horiuchi, P. Schuck, G. Röpke, [Alpha cluster condensation in  \$^{12}\text{C}\$  and  \$^{16}\text{O}\$](#) , Phys. Rev. Lett. 87 (2001) 192501.
- [33] E. Epelbaum, H. Krebs, D. Lee, U.-G. Meissner, [Ab initio calculation of the hoyle state](#), Phys. Rev. Lett. 106 (2011) 192501.
- [34] E. Epelbaum, H. Krebs, T. A. Lähde, D. Lee, U.-G. Meissner, [Structure and rotations of the hoyle state](#), Phys. Rev. Lett. 109 (2012) 252501.
- [35] B. Zhou, A. Tohsaki, H. Horiuchi, Z. Ren, [Breathing-like excited state of the hoyle state in  \$^{12}\text{C}\$](#) , Phys. Rev. C 94 (2016) 044319.
- [36] N. Itagaki, T. Otsuka, K. Ikeda, S. Okabe, [Equilateral-triangular shape in  \$^{14}\text{C}\$](#) , Phys. Rev. Lett. 92 (2004) 142501.
- [37] N. Furutachi, M. Kimura, [Bent three- \$\alpha\$  linear-chain structure of  \$^{13}\text{C}\$](#) , Phys. Rev. C 83 (2011) 021303(R).
- [38] T. Suhara, Y. Kanada-En'yo, [Cluster structures of excited states in  \$^{14}\text{C}\$](#) , Phys. Rev. C 82 (2010) 044301.
- [39] T. Baba, Y. Chiba, M. Kimura, [3 \$\alpha\$  clustering in excited states of  \$^{16}\text{C}\$](#) , Phys. Rev. C 90 (2014) 064319.
- [40] G. R. Jansen, J. Engel, G. Hagen, P. Navratil, A. Signoracci, [Ab initio coupled-cluster effective interactions for the shell model: Application to neutron-rich oxygen and carbon isotopes](#), Phys. Rev. Lett. 113 (2014) 142502.
- [41] M. Freer, H. Horiuchi, Y. Kanada-En'yo, D. Lee, U.-G. Meissner, [Microscopic clustering in light nuclei](#), Rev. Mod. Phys. 90 (2018) 035004.
- [42] Z. Y. Tian, Y. L. Ye, Z. H. Li, C. J. Lin, Q. T. Li, Y. C. Ge, J. L. Lou, W. Jiang, J. Li, Z. H. Yang, J. Feng, P. J. Li, J. Chen, Q. Liu, H. L. Zang, B. Yang, Y. Zhang, Z. Q. Chen, Y. Liu, X. H. Sun, J. Ma, H. M. Jia, X. X. Xu, L. Yang, N. R. Ma, L. J. Sun, [Cluster decay of the high-lying excited states in  \$^{14}\text{C}\$](#) , Chin. Phys. C 40 (11) (2016) 111001.

- [43] J. Li, Y. L. Ye, Z. H. Li, C. J. Lin, Q. T. Li, Y. C. Ge, J. L. Lou, Z. Y. Tian, W. Jiang, Z. H. Yang, J. Feng, P. J. Li, J. Chen, Q. Liu, H. L. Zang, B. Yang, Y. Zhang, Z. Q. Chen, Y. Liu, X. H. Sun, J. Ma, H. M. Jia, X. X. Xu, L. Yang, N. R. Ma, L. J. Sun, [Selective decay from a candidate of the  \$\sigma\$ -bond linear-chain state in  \$^{14}\text{C}\$](#) , Phys. Rev. C 95 (2017) 021303(R).
- [44] Z. Ren, S. Zhang, P. Zhao, N. Itagaki, J. A. Maruhn, J. Meng, [Stability of the linear chain structure for  \$^{12}\text{C}\$  in covariant density functional theory on a 3D lattice](#), Sci. China-Phys. Mech. Astron. 62 (11) (2019) 112062.
- [45] P. W. Zhao, N. Itagaki, J. Meng, [Rod-shaped nuclei at extreme spin and isospin](#), Phys. Rev. Lett. 115 (2015) 022501.
- [46] W. Pöschl, D. Vretenar, G. A. Lalazissis, P. Ring, [Relativistic Hartree-Bogoliubov theory with finite range pairing forces in coordinate space: Neutron halo in light nuclei](#), Phys. Rev. Lett. 79 (1997) 3841.
- [47] X. L. Lu, B. Y. Sun, W. H. Long, [Description of carbon isotopes within relativistic Hartree-Fock-Bogoliubov theory](#), Phys. Rev. C 87 (2013) 034311.
- [48] M. M. Sharma, S. Mythili, A. R. Farhan, [Carbon isotopes near drip lines in the relativistic mean-field theory](#), Phys. Rev. C 59 (1999) 1379–1390.
- [49] G. A. Lalazissis, D. Vretenar, P. Ring, [Relativistic Hartree-Bogoliubov description of deformed light nuclei](#), Eur. Phys. J. A 22 (1) (2004) 37–45.
- [50] W.-Z. Jiang, Z.-Z. Ren, Z.-Y. Zhu, T.-T. Wang, Z.-J. He, [Exotic structures of odd-A Carbon isotopes in the deformed relativistic mean-field theory](#), Commun. Theor. Phys. 41 (1) (2004) 79–82.
- [51] B.-N. Lu, E.-G. Zhao, S.-G. Zhou, [Quadrupole deformation \( \$\beta, \gamma\$ \) of light  \$\Lambda\$  hypernuclei in a constrained relativistic mean field model: Shape evolution and shape polarization effect of the  \$\Lambda\$  hyperon](#), Phys. Rev. C 84 (2011) 014328.

- [52] J. M. Yao, J. Meng, P. Ring, Z. X. Li, Z. P. Li, K. Hagino, [Microscopic description of quantum shape fluctuation in C isotopes](#), Phys. Rev. C 84 (2011) 024306.
- [53] H. Sagawa, X. R. Zhou, X. Z. Zhang, T. Suzuki, [Deformations and electromagnetic moments in carbon and neon isotopes](#), Phys. Rev. C 70 (2004) 054316.
- [54] Y. Kanada-En'yo, [Deformation of C isotopes](#), Phys. Rev. C 71 (2005) 014310.
- [55] Y. Zhang, H. Sagawa, D. Yoshino, K. Hagino, J. Meng, [Shape evolution of C isotopes in  \$\(\beta, \gamma\)\$  deformation plane](#), Prog. Theor. Phys. 120 (1) (2008) 129–142.
- [56] C. Yuan, T. Suzuki, T. Otsuka, F. Xu, N. Tsunoda, [Shell-model study of boron, carbon, nitrogen, and oxygen isotopes with a monopole-based universal interaction](#), Phys. Rev. C 85 (2012) 064324.
- [57] S.-G. Zhou, [Structure of Exotic Nuclei: A Theoretical Review](#), PoS INPC2016 (2017) 373.
- [58] X.-X. Sun, J. Zhao, S.-G. Zhou, [Shrunk halo and quenched shell gap at  \$N = 16\$  in  \$^{22}\text{C}\$ : Inversion of  \$sd\$  states and deformation effects](#), Phys. Lett. B 785 (2018) 530–535.
- [59] S.-G. Zhou, J. Meng, P. Ring, E.-G. Zhao, [Neutron halo in deformed nuclei](#), Phys. Rev. C 82 (2010) 011301(R).
- [60] L. Li, J. Meng, P. Ring, E.-G. Zhao, S.-G. Zhou, [Deformed relativistic Hartree-Bogoliubov theory in continuum](#), Phys. Rev. C 85 (2012) 024312.
- [61] L.-L. Li, J. Meng, P. Ring, E.-G. Zhao, S.-G. Zhou, [Odd systems in deformed relativistic Hartree-Bogoliubov theory in continuum](#), Chin. Phys. Lett. 29 (4) (2012) 042101.
- [62] J. Meng, S.-G. Zhou, [Halos in medium-heavy and heavy nuclei with covariant density functional theory in continuum](#), J. Phys. G: Nucl. Part. Phys. 42 (9) (2015) 093101.

- [63] K. Y. Zhang, D. Y. Wang, S. Q. Zhang, [Effects of pairing, continuum, and deformation on particles in the classically forbidden regions for Mg isotopes](#), Phys. Rev. C 100 (2019) 034312.
- [64] K. Zhang, M.-K. Cheoun, Y.-B. Choi, P. S. Chong, J. Dong, L. Geng, E. Ha, X. He, C. Heo, M. C. Ho, E. J. In, S. Kim, Y. Kim, C.-H. Lee, J. Lee, Z. Li, T. Luo, J. Meng, M.-H. Mun, Z. Niu, C. Pan, P. Papakonstantinou, X. Shang, C. Shen, G. Shen, W. Sun, X.-X. Sun, C. K. Tam, Thaivayongnou, C. Wang, S. H. Wong, X. Xia, Y. Yan, R. W.-Y. Yeung, T. C. Yiu, S. Zhang, W. Zhang, S.-G. Zhou, [Toward a nuclear mass table with the continuum and deformation effects: even-even nuclei in the nuclear chart](#), arXiv:2001.06599 [nucl-th].
- [65] J. C. Pei, Y. N. Zhang, F. R. Xu, [Evolution of surface deformations of weakly bound nuclei in the continuum](#), Phys. Rev. C 87 (2013) 051302(R).
- [66] J. C. Pei, M. Kortelainen, Y. N. Zhang, F. R. Xu, [Emergent soft monopole modes in weakly bound deformed nuclei](#), Phys. Rev. C 90 (2014) 051304(R).
- [67] X.-Y. Xiong, J.-C. Pei, Y.-N. Zhang, Y. Zhu, Study of weakly-bound odd- $A$  nuclei with quasiparticle blocking, Chin. Phys. C 40 (2) (2016) 024101.
- [68] K. Wang, M. Kortelainen, J. C. Pei, [Probing surface quantum flows in deformed pygmy dipole modes](#), Phys. Rev. C 96 (2017) 031301(R).
- [69] H. Nakada, [Semi-realistic nucleon-nucleon interactions with improved neutron-matter properties](#), Phys. Rev. C 87 (2013) 014336.
- [70] H. Nakada, K. Takayama, [Intertwined effects of pairing and deformation on neutron halos in magnesium isotopes](#), Phys. Rev. C 98 (2018) 011301(R).
- [71] B. Serot, J. Walecka, The relativistic nuclear many-body problem, Adv. Nucl. Phys. 16 (1986) 1–327.
- [72] P. G. Reinhard, [The relativistic mean-field description of nuclei and nuclear dynamics](#), Rep. Prog. Phys. 52 (4) (1989) 439.

- [73] P. Ring, [Relativistic mean field theory in finite nuclei](#), Prog. Part. Nucl. Phys. 37 (0) (1996) 193–263.
- [74] D. Vretenar, A. V. Afanasjev, G. A. Lalazissis, P. Ring, [Relativistic Hartree-Bogoliubov theory: static and dynamic aspects of exotic nuclear structure](#), Phys. Rep. 409 (3–4) (2005) 101–259.
- [75] J. Meng, H. Toki, S. Zhou, S. Zhang, W. Long, L. Geng, [Relativistic continuum Hartree-Bogoliubov theory for ground-state properties of exotic nuclei](#), Prog. Part. Nucl. Phys. 57 (2) (2006) 470–563.
- [76] T. Nikšić, D. Vretenar, P. Ring, [Relativistic nuclear energy density functionals: Mean-field and beyond](#), Prog. Part. Nucl. Phys. 66 (3) (2011) 519–548.
- [77] J. Meng, J. Peng, S.-Q. Zhang, P.-W. Zhao, [Progress on tilted axis cranking covariant density functional theory for nuclear magnetic and antimagnetic rotation](#), Front. Phys. 8 (1) (2013) 55–79.
- [78] H. Liang, J. Meng, S.-G. Zhou, [Hidden pseudospin and spin symmetries and their origins in atomic nuclei](#), Phys. Rep. 570 (2015) 1–84.
- [79] J. Meng (Ed.), [Relativistic Density Functional for Nuclear Structure](#), World Scientific, 2016.
- [80] J. Meng, P. Ring, [Relativistic Hartree-Bogoliubov description of the neutron halo in  \$^{11}\text{Li}\$](#) , Phys. Rev. Lett. 77 (1996) 3963–3966.
- [81] J. Meng, [Relativistic continuum Hartree-Bogoliubov theory with both zero range and finite range Gogny force and their application](#), Nucl. Phys. A 635 (1–2) (1998) 3–42.
- [82] Y. Chen, L. Li, H. Liang, J. Meng, [Density-dependent deformed relativistic Hartree-Bogoliubov theory in continuum](#), Phys. Rev. C 85 (2012) 067301.
- [83] H. Kucharek, P. Ring, [Relativistic field theory of superfluidity in nuclei](#), Z. Phys. A 339 (1) (1991) 23–35.
- [84] S.-G. Zhou, J. Meng, P. Ring, [Spherical relativistic Hartree theory in a Woods-Saxon basis](#), Phys. Rev. C 68 (2003) 034323.

- [85] P. Ring, P. Schuck, [The Nuclear Many-Body Problem](#), Springer-Verlag Berlin Heidelberg, 1980.
- [86] J. P. Blaizot, G. Ripka, [Quantum Theory of Finite Systems](#), The MIT Press, 1985.
- [87] A. Staszczak, M. Stoitsov, A. Baran, W. Nazarewicz, [Augmented Lagrangian method for constrained nuclear density functional theory](#), Eur. Phys. J. A 46 (1) (2010) 85–90.
- [88] Y. Chen, P. Ring, J. Meng, [Influence of pairing correlations on the size of the nucleus in relativistic continuum Hartree-Bogoliubov theory](#), Phys. Rev. C 89 (2014) 014312.
- [89] J. Dobaczewski, H. Flocard, J. Treiner, [Hartree-Fock-Bogolyubov description of nuclei near the neutron-drip line](#), Nucl. Phys. A 422 (1) (1984) 103–139.
- [90] W. Long, J. Meng, N. V. Giai, S.-G. Zhou, [New effective interactions in relativistic mean field theory with nonlinear terms and density-dependent meson-nucleon coupling](#), Phys. Rev. C 69 (2004) 034319.
- [91] G. A. Lalazissis, J. König, P. Ring, [New parametrization for the Lagrangian density of relativistic mean field theory](#), Phys. Rev. C 55 (1997) 540–543.
- [92] B. Pritychenko, M. Birch, B. Singh, M. Horoi, [Tables of E2 transition probabilities from the first  \$2^+\$  states in even-even nuclei](#), At. Data Nucl. Data Tables 107 (2016) 1–139.
- [93] M. Yasue, T. Tanabe, F. Soga, J. Kokame, F. Shimokoshi, J. Kasagi, Y. Toba, Y. Kadota, T. Ohsawa, K. Furuno, [Deformation parameter of  \$^{12}\text{C}\$  via  \$^{12}\text{C}\(\alpha, \alpha'\)\$  and  \$^{12}\text{C}\(\alpha, \alpha'\alpha\)\$  reactions](#), Nucl. Phys. A 394 (1) (1983) 29–38.
- [94] Y. Jiang, J. L. Lou, Y. L. Ye, Y. Liu, Z. W. Tan, W. Liu, B. Yang, L. C. Tao, K. Ma, Z. H. Li, Q. T. Li, X. F. Yang, J. Y. Xu, H. Z. Yu, J. X. Han, S. W. Bai, S. W. Huang, G. Li, H. Y. Wu, H. L. Zang, J. Feng, Z. Q. Chen, Y. D. Chen, Q. Yuan, J. G. Li, B. S. Hu, F. R. Xu, J. S. Wang, Y. Y. Yang, P. Ma, Q. Hu, Z. Bai, Z. H. Gao, F. F. Duan, L. Y. Hu, J. H. Tan, S. Q. Sun, Y. S. Song, H. J. Ong, D. T.

- Tran, D. Y. Pang, C. X. Yuan, [Quadrupole deformation of  \$^{16}\text{C}\$  studied by proton and deuteron inelastic scattering](#), Phys. Rev. C 101 (2020) 024601.
- [95] Z. Elekes, Z. Dombrádi, R. Kanungo, H. Baba, Z. Fülöp, J. Gibelin, A. Horváth, E. Ideguchi, Y. Ichikawa, N. Iwasa, H. Iwasaki, S. Kanno, S. Kawai, Y. Kondo, T. Motobayashi, M. Notani, T. Ohnishi, A. Ozawa, H. Sakurai, S. Shimoura, E. Takeshita, S. Takeuchi, I. Tanihata, Y. Togano, C. Wu, Y. Yamaguchi, Y. Yanagisawa, A. Yoshida, K. Yoshida, [Low-lying excited states in  \$^{17,19}\text{C}\$](#) , Phys. Lett. B 614 (3) (2005) 174–180.
- [96] M. Zhukov, B. Danilin, D. Fedorov, J. Bang, I. Thompson, J. Vaagen, [Bound state properties of borromean halo nuclei:  \$^6\text{He}\$  and  \$^{11}\text{Li}\$](#) , Phys. Rep. 231 (4) (1993) 151–199.
- [97] H. T. Fortune, [Update on matter radii of carbon nuclei](#), Phys. Rev. C 94 (2016) 064307.
- [98] M. K. Raju, J. Orice, P. Navrátil, G. Ball, T. Drake, S. Triambak, G. Hackman, C. Pearson, K. Abrahams, E. Akakpo, H. A. Falou, R. Churchman, D. Cross, M. Djongolov, N. Erasmus, P. Finlay, A. Garnsworthy, P. Garrett, D. Jenkins, R. Kshetri, K. Leach, S. Masango, D. Mavela, C. Mehl, M. Mokgolobotho, C. Ngwetsheni, G. O’Neill, E. Rand, S. Sjue, C. Sumithrarachchi, C. Svensson, E. Tardiff, S. Williams, J. Wong, [Reorientation-effect measurement of the first  \$2^+\$  state in  \$^{12}\text{C}\$ : Confirmation of oblate deformation](#), Phys. Lett. B 777 (2018) 250–254.
- [99] H. Sagawa, X. R. Zhou, T. Suzuki, N. Yoshida, [Possible shape coexistence and magnetic dipole transitions in  \$^{17}\text{C}\$  and  \$^{21}\text{Ne}\$](#) , Phys. Rev. C 78 (2008) 041304(R).
- [100] M. J. Strongman, A. Spyrou, C. R. Hoffman, T. Baumann, D. Bazin, J. Brown, P. A. DeYoung, J. E. Finck, N. Frank, S. Mosby, W. F. Rogers, G. F. Peaslee, W. A. Peters, A. Schiller, S. L. Tabor, M. Thoennessen, [Disappearance of the  \$N = 14\$  shell](#), Phys. Rev. C 80 (2009) 021302(R).



- [101] U. D. Pramanik, T. Aumann, K. Boretzky, B. Carlson, D. Cortina, T. Elze, H. Emling, H. Geissel, A. Grünscho, M. Hellström, S. Ilievski, J. Kratz, R. Kulesa, Y. Leifels, A. Leistenschneider, E. Lubkiewicz, G. Münzenberg, P. Reiter, H. Simon, K. Sümmerer, E. Wajda, W. Walus, [Coulomb breakup of the neutron-rich isotopes  \$^{15}\text{C}\$  and  \$^{17}\text{C}\$](#) , Phys. Lett. B 551 (2003) 63–70.
- [102] G. Murillo, S. Sen, S. Darden, [A study of the reactions  \$^{14}\text{C}\(\vec{d}, d'\)^{14}\text{C}\$  and  \$^{14}\text{C}\(\vec{d}, p\)^{15}\text{C}\$  at 16.0 MeV](#), Nucl. Phys. A 579 (1-2) (1994) 125–143.
- [103] J. R. Terry, D. Bazin, B. A. Brown, J. Enders, T. Glasmacher, P. G. Hansen, B. M. Sherrill, J. A. Tostevin, [Absolute spectroscopic factors from neutron knockout on the halo nucleus  \$^{15}\text{C}\$](#) , Phys. Rev. C 69 (2004) 054306.
- [104] V. Maddalena, T. Aumann, D. Bazin, B. A. Brown, J. A. Caggiano, B. Davids, T. Glasmacher, P. G. Hansen, R. W. Ibbotson, A. Navin, B. V. Pritychenko, H. Scheit, B. M. Sherrill, M. Steiner, J. A. Tostevin, J. Yurkon, [Single-neutron knockout reactions: Application to the spectroscopy of  \$^{16,17,19}\text{C}\$](#) , Phys. Rev. C 63 (2001) 024613.
- [105] H. Ueno, H. Miyatake, Y. Yamamoto, S. Tanimoto, T. Shimoda, N. Aoi, K. Asahi, E. Ideguchi, M. Ishihara, H. Izumi, T. Kishida, T. Kubo, S. Mitsuoka, Y. Mizoi, M. Notani, H. Ogawa, A. Ozawa, M. Sasaki, T. Shirakura, N. Takahashi, K. Yoneda,  [\$\beta\$ -delayed neutron and  \$\gamma\$ -ray spectroscopy of  \$^{17}\text{C}\$  utilizing spin-polarized  \$^{17}\text{B}\$](#) , Phys. Rev. C 87 (2013) 034316.
- [106] T. Nakamura, N. Fukuda, T. Kobayashi, N. Aoi, H. Iwasaki, T. Kubo, A. Mengoni, M. Notani, H. Otsu, H. Sakurai, S. Shimoura, T. Teranishi, Y. X. Watanabe, K. Yoneda, M. Ishihara, [Coulomb dissociation of  \$^{19}\text{C}\$  and its halo structure](#), Phys. Rev. Lett. 83 (1999) 1112–1115.
- [107] J. Hwang, S. Kim, Y. Satou, N. Orr, Y. Kondo, T. Nakamura, J. Gibelin, N. Achouri, T. Aumann, H. Baba, F. Delaunay, P. Doornenbal, N. Fukuda, N. Inabe, T. Isobe, D. Kameda, D. Kanno, N. Kobayashi, T. Kobayashi, T. Kubo, S. Leblond, J. Lee, F. Marquš, R. Minakata, T. Motobayashi, D. Murai, T. Murakami, K. Muto,

- T. Nakashima, N. Nakatsuka, A. Navin, S. Nishi, S. Ogoshi, H. Otsu, H. Sato, Y. Shimizu, H. Suzuki, K. Takahashi, H. Takeda, S. Takeuchi, R. Tanaka, Y. Togano, A. Tuff, M. Vandebrout, K. Yoneda, [Single-neutron knockout from  \$^{20}\text{C}\$  and the structure of  \$^{19}\text{C}\$](#) , Phys. Lett. B 769 (2017) 503–508.
- [108] P. G. Hansen, B. Jonson, [The neutron halo of extremely neutron-rich nuclei](#), Europhys. Lett. 4 (4) (1987) 409.
- [109] J. Dobaczewski, W. Nazarewicz, T. R. Werner, J. F. Berger, C. R. Chinn, J. Dechargé, [Mean-field description of ground-state properties of drip-line nuclei: Pairing and continuum effects](#), Phys. Rev. C 53 (1996) 2809–2840.
- [110] J. Meng, P. Ring, [Giant halo at the neutron drip line](#), Phys. Rev. Lett. 80 (1998) 460–463.
- [111] A. S. Jensen, K. Riisager, D. V. Fedorov, E. Garrido, [Structure and reactions of quantum halos](#), Rev. Mod. Phys. 76 (2004) 215–261.
- [112] K. Riisager, [Halos and related structures](#), Phys. Scr. 2013 (T152) (2013) 014001.
- [113] S.-S. Zhang, M. S. Smith, Z.-S. Kang, J. Zhao, [Microscopic self-consistent study of neon halos with resonant contributions](#), Phys. Lett. B 730 (2014) 30–35.
- [114] Y. Zhang, Y. Chen, J. Meng, P. Ring, [Influence of pairing correlations on the radius of neutron-rich nuclei](#), Phys. Rev. C 95 (2017) 014316.
- [115] H. Sagawa, [Density distributions of halo nuclei](#), Phys. Lett. B 286 (1) (1992) 7–12.
- [116] M. J. G. Borge, H. Fynbo, D. Guillemaud-Mueller, P. Hornshøj, F. Humbert, B. Jonson, T. E. Leth, G. Martínez-Pinedo, T. Nilsson, G. Nyman, A. Poves, I. Ramos-Lerate, K. Riisager, G. Schrieder, M. Smedberg, O. Tengblad, [Elucidating halo structure by  \$\beta\$  decay:  \$\beta\gamma\$  from the  \$^{11}\text{Li}\$  decay](#), Phys. Rev. C 55 (1997) R8–R11.
- [117] D. Morrissey, K. McDonald, D. Bazin, B. Brown, R. Harkewicz, N. Orr, B. Sherrill, G. Souliotis, M. Steiner, J. Winger, S. Yennello, B. Young,

- S. Lukyanov, G. Chubarian, Y. Oganessian, [Single neutron emission following  \$^{11}\text{Li}\$   \$\beta\$ -decay](#), Nucl. Phys. A 627 (2) (1997) 222–238.
- [118] T. Misu, W. Nazarewicz, S. Åberg, [Deformed nuclear halos](#), Nucl. Phys. A 614 (1) (1997) 44–70.
- [119] J. Braun, H. W. Hammer, L. Platter, [Halo structure of  \$^{17}\text{C}\$](#) , Eur. Phys. J. A 54 (11) (2018) 196.
- [120] S.-G. Zhou, C. Zheng, J. Hu, [Configuration dependence of moments of inertia in the odd- \$A\$  nucleus from BCS theory](#), Phys. Rev. C 63 (2001) 047305.
- [121] D. Ridikas, M. H. Smedberg, J. S. Vaagen, M. V. Zhukov,  [\$^{19}\text{C}\$ : the heaviest one-neutron halo nucleus?](#), Europhys. Lett. 37 (6) (1997) 385.
- [122] R. Kanungo, I. Tanihata, Y. Ogawa, H. Toki, A. Ozawa, [Halo structure in  \$^{19}\text{C}\$ : A Glauber model analysis](#), Nucl. Phys. A 677 (1-4) (2000) 171–186.
- [123] B. Gönül, M. Yilmaz, [Halo structure of  \$^{19}\text{C}\$  via the \(p,d\) reaction](#), Few-Body Syst. 30 (3) (2001) 211–221.
- [124] J. Wang, W. Shen, Z. Zhu, J. Feng, Z. Guo, W. Zhan, G. Xiao, X. Cai, D. Fang, H. Zhang, Y. Ma, [RMF calculation and phenomenological formulas for the rms radii of light nuclei](#), Nucl. Phys. A 691 (3) (2001) 618–630.
- [125] B. Acharya, D. R. Phillips,  [\$^{19}\text{C}\$  in halo EFT: Effective-range parameters from coulomb dissociation experiments](#), Nucl. Phys. A 913 (2013) 103–115.
- [126] Y. Satou, T. Nakamura, N. Fukuda, T. Sugimoto, Y. Kondo, N. Matsui, Y. Hashimoto, T. Nakabayashi, T. Okumura, M. Shinohara, T. Motobayashi, Y. Yanagisawa, N. Aoi, S. Takeuchi, T. Gomi, Y. Togano, S. Kawai, H. Sakurai, H. Ong, T. Onishi, S. Shimoura, M. Tamaki, T. Kobayashi, H. Otsu, Y. Matsuda, N. Endo, M. Kitayama, M. Ishihara, [Unbound excited states in  \$^{19,17}\text{C}\$](#) , Phys. Lett. B 660 (4) (2008) 320–325.

- [127] T. Suzuki, H. Sagawa, K. Hagino, [Exotic structure of carbon isotopes](#), in: H. Sagawa, H. Iwasaki (Eds.), Proceedings of the International Symposium on Frontiers of Collective Motions (CM2002), World Scientific, 2003, p. 236.
- [128] X.-N. Cao, Q. Liu, J.-Y. Guo, [Interpretation of halo in  \$^{19}\text{C}\$  with complex momentum representation method](#), J. Phys. G: Nucl. Part. Phys. 45 (8) (2018) 085105.
- [129] B. Abu-Ibrahim, W. Horiuchi, A. Kohama, Y. Suzuki, [Reaction cross sections of carbon isotopes incident on a proton](#), Phys. Rev. C 77 (2008) 034607.
- [130] B. Abu-Ibrahim, W. Horiuchi, A. Kohama, Y. Suzuki, [Publisher’s note: Reaction cross sections of carbon isotopes incident on a proton \[Phys. Rev. C 77, 034607 \(2008\)\]](#), Phys. Rev. C 81 (2010) 019901.
- [131] B. Abu-Ibrahim, W. Horiuchi, A. Kohama, Y. Suzuki, [Erratum: Reaction cross sections of carbon isotopes incident on a proton \[Phys. Rev. C 77, 034607 \(2008\)\]](#), Phys. Rev. C 80 (2009) 029903.
- [132] M. Yamashita, R. M. de Carvalho, T. Frederico, L. Tomio, [Constraints on two-neutron separation energy in the Borromean  \$^{22}\text{C}\$  nucleus](#), Phys. Lett. B 697 (1) (2011) 90–93.
- [133] H. T. Fortune, R. Sherr, [Binding energy of  \$^{22}\text{C}\$](#) , Phys. Rev. C 85 (2012) 027303.
- [134] S. N. Ershov, J. S. Vaagen, M. V. Zhukov, [Binding energy constraint on matter radius and soft dipole excitations of  \$^{22}\text{C}\$](#) , Phys. Rev. C 86 (2012) 034331.
- [135] N. B. Shulgina, S. N. Ershov, J. S. Vaagen, M. V. Zhukov, [Superhalo of  \$^{22}\text{C}\$  reexamined](#), Phys. Rev. C 97 (2018) 064307.
- [136] N. Kobayashi, T. Nakamura, J. A. Tostevin, Y. Kondo, N. Aoi, H. Baba, S. Deguchi, J. Gibelin, M. Ishihara, Y. Kawada, T. Kubo, T. Motobayashi, T. Ohnishi, N. A. Orr, H. Otsu, H. Sakurai, Y. Satou, E. C. Simpson, T. Sumikama, H. Takeda, M. Takechi, S. Takeuchi, K. N. Tanaka, N. Tanaka, Y. Togano, K. Yoneda, [One- and two-neutron](#)

- removal reactions from the most neutron-rich carbon isotopes, *Phys. Rev. C* 86 (2012) 054604.
- [137] T. Frederico, A. Delfino, L. Tomio, M. Yamashita, [Universal aspects of light halo nuclei](#), *Prog. Part. Nucl. Phys.* 67 (4) (2012) 939–994.
  - [138] P. Hagen, H. W. Hammer, L. Platter, [Charge form factors of two-neutron halo nuclei in halo EFT](#), *Eur. Phys. J. A* 49 (9) (2013) 118.
  - [139] K. Ogata, T. Myo, T. Furumoto, T. Matsumoto, M. Yahiro, [Interplay between the  \$0\_2^+\$  resonance and the nonresonant continuum of the drip-line two-neutron halo nucleus  \$^{22}\text{C}\$](#) , *Phys. Rev. C* 88 (2013) 024616.
  - [140] B. Acharya, C. Ji, D. Phillips, [Implications of a matter-radius measurement for the structure of  \$^{22}\text{C}\$](#) , *Phys. Lett. B* 723 (2013) 196–200.
  - [141] Y. Kucuk, J. A. Tostevin, [Intermediate-energy four-body breakup calculations for  \$^{22}\text{C}\$](#) , *Phys. Rev. C* 89 (3) (2014) 034607.
  - [142] C. R. Hoffman, B. P. Kay, J. P. Schiffer, [Neutron  \$s\$  states in loosely bound nuclei](#), *Phys. Rev. C* 89 (2014) 061305(R).
  - [143] T. Inakura, W. Horiuchi, Y. Suzuki, T. Nakatsukasa, [Mean-field analysis of ground-state and low-lying electric dipole strength in  \$^{22}\text{C}\$](#) , *Phys. Rev. C* 89 (2014) 064316.
  - [144] C. Ji, [Three-body systems in physics of cold atoms and halo nuclei](#), *Int. J. Mod. Phys. E* 25 (05) (2016) 1641003.
  - [145] E. C. Pinilla, P. Descouvemont, [Coulomb breakup of  \$^{22}\text{C}\$  in a four-body model](#), *Phys. Rev. C* 94 (2016) 024620.
  - [146] L. A. Souza, E. Garrido, T. Frederico, [Emergent universality in the two-neutron halo structure of  \$^{22}\text{C}\$](#) , *Phys. Rev. C* 94 (2016) 064002.
  - [147] T. Suzuki, T. Otsuka, C. Yuan, N. Alahari, [Two-neutron halo from the low-energy limit of neutron-neutron interaction: Applications to drip-line nuclei  \$^{22}\text{C}\$  and  \$^{24}\text{O}\$](#) , *Phys. Lett. B* 753 (2016) 199–203.

- [148] L. Souza, F. Bellotti, M. Yamashita, T. Frederico, L. Tomio, [Core momentum distribution in two-neutron halo nuclei](#), Phys. Lett. B 757 (2016) 368–375.
- [149] H. Toki, D. Hirata, Y. Sugahara, K. Sumiyoshi, I. Tanihata, [Relativistic many body approach for unstable nuclei and supernova](#), Nucl. Phys. A 588 (1) (1995) c357–c363.
- [150] B. S. Hu, Q. Wu, Z. H. Sun, F. R. Xu, [Ab initio Gamow in-medium similarity renormalization group with resonance and continuum](#), Phys. Rev. C 99 (2019) 061302(R).